공학박사학위논문

Electric Potential Build-up by Trapped Electrons in Magnetically Expanding Plasma

자기적으로 팽창하는 플라즈마에서의 구속된 전자에 의한 양극성 전위 형성 연구

2020 년 1 월

서울대학교 대학원

에너지시스템공학부

정 경 수

Electric Potential Build-up by Trapped Electrons in Magnetically Expanding Plasma

자기적으로 팽창하는 플라즈마에서의 구속된 전자에 의한 양극성 전위 형성 연구

지도교수 황 용 석

이 논문을 공학박사 학위논문으로 제출함

2020 년 1 월

서울대학교 대학원
에너지시스템공학부
정 경 수

정경수의 공학박사 학위논문을 인준함

2020 년 1 월

위 원 장 정 경 재 (인)

부위원장 황 용 석 (인)

위 원 최 원 호 (인)

위 원 나 용 수 (인)

위 원 윤 건 수 (인)

Abstract

Electric Potential Build-up by Trapped Electrons in Magnetically Expanding Plasma

Kyoung Soo Chung

Department of Energy System Engineering

The Graduate School

Seoul National University

A magnetic nozzle leads the ion beam accelerated by the adiabatic expansion of plasma electrons in the expanding magnetic field for thrust. This concept has the advantage that the expanding electrons can be directly used for the neutralization of the ion beam without additional installation of a cathode for neutralizing the ion beam. Then, it is discussed as the next generation electric thruster. The efficiency of the magnetic nozzle apparatus in terms of ion beam acceleration energy is determined by the relationship between electron cooling and plasma potential gradient via a polytropic equation that can represent the adiabatic expansion in magnetically expanding plasma. Thus, previous studies have been conducted with the importance that a clear understanding of the electron thermodynamics in the magnetic nozzle contributes to the thrust efficiency.

For the analysis of the electron thermodynamic state in the magnetic nozzle plasma, it describes the magnetically expanding plasma by introducing a total energy conservation law in which changes in the internal energy of the electron gas system work on magnetic and electric fields defined as flexible surroundings. The experiment and modeling results for the electron thermodynamics indicate that the system is enable to be classified based on the electron group trapped by the electric potential barrier or constant maximum magnetic moment. In the case of electrically trapped electrons, the adiabatic expansion of the electrons contributes to the formation of the electric field structure, while escaping electrons may work to cause a change in the magnetic field structure regardless of the electric field formation. Hence, in the electron thermodynamics of the magnetic nozzle plasma, it implies that consideration of the electrostatic confinement is essential. Previous studies focused on the identification of the electron thermodynamic states based on a clear definition of the electron gas system have been the basis for studying the relationship between the electron thermodynamics and the efficiency of magnetic nozzles, and require refined study that reflect complex plasma physics.

Notice that the plasma generation in the magnetic nozzle apparatus is achieved by the electron energy and directional selective heating on them, it is emphasized that the study on the plasma potential gradient formation due to the change of the thermodynamic state of the electrons should be carried out based on the diagnosis considering the directional orientation of the electrons. The electron energy distribution function (EEDF) of each directional component is measured, while increasing the applied power to the plasma source by electron cyclotron resonance (ECR), and selectively changing the perpendicular electron energy. Interestingly, the increase in the perpendicular energy of the electrons at the nozzle throat did not contribute to the formation of the plasma potential gradient, which is interpreted because most of the power applied for the electron heating contributed to the rise in the perpendicular energy of the escaping electrons. In the case of the electron energy in the parallel direction, the electron heating in the far-field region of the nozzle is observed as the applied power increased, and this heating induces the synergistic effect of the absolute value of the plasma potential, resulting in the attenuation of the ambipolar electric field generated by the trapped electron group in the perpendicular direction. The correlation

between the plasma potential gradient change and the change of electron cooling and energy transfer from perpendicular to parallel component of the trapped electrons according to the applied power proves that the trapped electrons contribute to the electric field formation through the adiabatic expansion and suggests the following points. First, heating of trapped electrons directly contributes to the build-up of an electric field for ion acceleration in a magnetic nozzle utilizing ECR heating. Second, the change in the paraxial thermal energy of the trapped electrons and the change in the electric field are demonstrated by the adiabatic expansion of which the polytropic index is close to 5/3. Third, the electron energy transfer between the perpendicular and parallel directions can interrupt formation of the electric field in far-field region. Therefore, modeling and device design in the magnetic nozzle research that reflects the above perspectives are essential.

This study is the first to emphasize that the anisotropy of electron temperature can directly affect the magnetic nozzle efficiency when generating magnetic nozzle plasma by wave heating. From the engineering point of view, it is important that the ratio of trapped electrons should be prioritized to abundant via plasma potential control for efficient increase of ion energy. Through the further research on the plasma generation method such as parallel electron energy heating in the plasma generation region, this suggests that energy conversion from the perpendicular to the parallel direction due to magnetic expansion in the far-field region can be minimized.

keywords : Magnetic nozzle, Polytropic index, Electron cooling, Directional Langmuir probe, Anisotropic electron energy distribution, Ambipolar electric potential

student number : 2013-30295

Contents

List of Tables

List of Figures

Chapter 1 Introduction

An electric propulsion is a kind of space propulsion that uses electrical power to accelerate propellants by different electric and/or magnetic means [1-3]. The use of power improves the propulsion performance of electric propulsion thrusters compared to conventional chemical thrusters. Unlike chemical systems, the electric thruster requires very little mass to accelerate the spacecraft [4-8]. The propellants are discharged up to 20 times faster than conventional chemical thrusters, and therefore the entire system is more efficient. The electric propulsion is not limited to energy compared to the chemical propulsion, but is only limited by the available power of the spacecraft. Therefore, electric thruster is suitable for long-term use and low thrust (micro and milli-newton levels) on board spacecrafts. The propellant used in the electric propulsion system depends on the type of thruster and can be rare gas (i.e. xenon or argon), liquid metal or in some cases conventional propulsion.

A gridded ion thruster and Hall thruster are electric propulsion system which are commonly used recently [9]. The two types of propulsion differ in the shape of the electrodes and the use of the grid for acceleration, as shown in Fig 1.1 [10]. Structurally, in the Hall thruster, unmagnetized ions are accelerated by an electric field between the anode and the cathode, while gridded ion thruster accelerates ions by applying a dc voltage to the electrode. The Hall thruster has a high propulsion density, and the gridded ion thruster has the advantage of producing high specific impulse. Table 1.1 summarizes the characteristics of each propulsion system. These types of the electric thruster yield relatively weak propulsion (0.01 N – 0.5 N), compared to the chemical propulsion, but produces a generally high propulsive efficiency, which is a specific impulse of more than 1000 s. The specific impulse here, is a standard of how much thrust is generated depending on the fuel consumed. However, these types of the electric thrusters have structures such as electrodes and grids, which make it difficult to minimize them. In addition, the damage to the materials those are the objects and the cathode for neutralization makes it is not possible to use in space missions for long periods of time.

To overcome the problems, the concept of a magnetic nozzle without using an electrode and a cathode for neutralization has begun to emerge. The role of the magnetic nozzle is transformation of the internal energy of the plasma into directed kinetic energy and plasma detachment which is comes out from the magnetic field. Recently, there has been great interest in area of physics and applications in magnetically expanding plasmas such as electric propulsion [4-9], space plasma physics [11-13], and plasma material processing [14-15]. In those area of the research, helicon and electron cyclotron resonance (ECR) discharges are mainly used to efficiency produce the plasma.

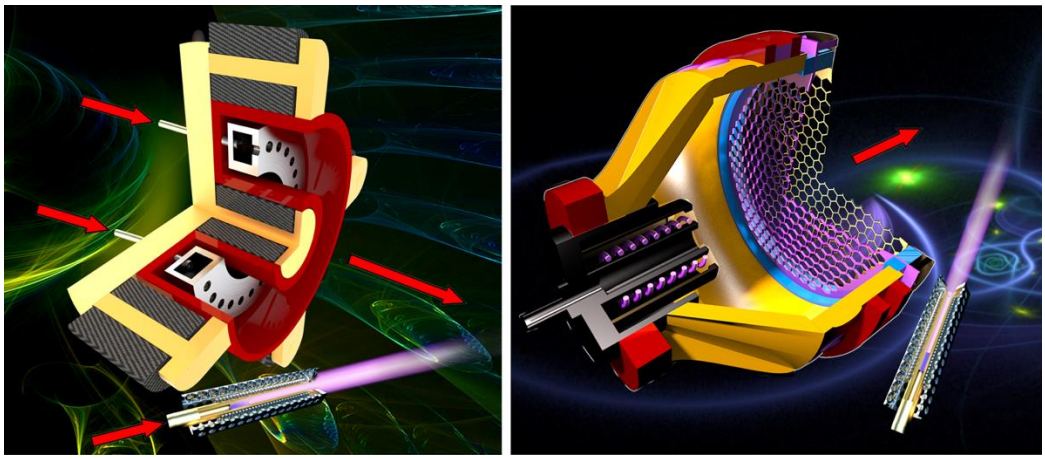

Figure 1.1 Schematic illustrations of Hall thruster (left), and Gridded ion thruster (right) [10]

Table 1.1 Hall thruster vs. Gridded ion thruster performance.

Characteristic	Hall effect thruster	Gridded ion thruster
Specific power	18 W/mN	25 - 35 W/mN
Thruster efficiency	50 %	70 %
Specific impulse	1500 - 2500 s	1500 - 2500 s
Operating voltage	300 - 400 V	1200 - 2000 V
Specific mass	5 kg/kW	10 kg/kW
Plume divergence	45˚	15˚
Throttle range	2:1	10:1

1.1 Ion Acceleration Mechanism in Magnetic Nozzle

The structural features of the magnetic nozzle [55, 56] are described with the principles of operation of a propulsive magnetic nozzle. As shown in Fig 1.2, the nozzle structure can be classified into three areas; 1) Plasma source region in which the plasma is generated, 2) Nozzle throat region conversed by the magnetic field of solenoid coils, 3) Expansion region in which the magnetic field diverges. The basic ideal operation is characterized by most of the internal energy being in the form of electron thermal energy, with electrons nearly isotropic and Maxwellian distribution. The set of solenoids conveniently placed generates the required converging-diverging magnetic field topology. The magnetic field is strong enough to magnetize electrons fully, but ion typically only partially. A quasi-neutral plasma is created in an upstream source and injected sonically and globally current-free at the nozzle throat into the expansion region. Efficient operation requires that the plasma be fully-ionized and collisionless. In this operation, no external electric fields are applied, no electric current flows into or out of the plasma through the thruster, and the plasma rotation is negligible.

The magnetized electrons then describe the geometry imposed by the magnetic field. Since the ions are not fully magnetized, they are not obliged to follow the magnetic field lines. An ambipolar electric field develops in the plasma in response to the expansion that performs several roles: perpendiculary to the magnetic field, the electric field compels ions to expand outward to maintain quasi-neutrality in the plasma domain; parallelly, it accelerates the ions downstream and confines most of the electrons upstream, with only a small tail of their distribution being able to surmount the potential jump and neutralize the ion beam. In this way, with the mediation of the electric field, the internal energy of electrons is transformed into directed kinetic energy of ions.

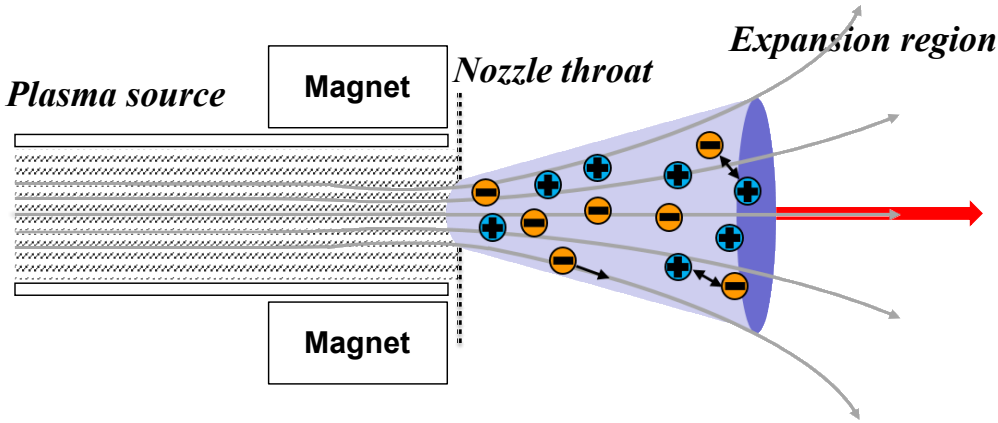

Figure 1.2 Structural features of magnetic nozzle.

The fundamental goal of magnetic nozzle is to achieve high propulsion efficiently. For this purpose, it is essential to understand the ion acceleration mechanism in the environment where the plasma moves in the magnetic field. In summary, the following issues are key to the acceleration of ions.

1) Generation in plasma source region
    - Plasma heating and transport to nozzle throat
2) Electron cooling process in an expanding magnetic field
    - Adiabatic expansion
3) Axial plasma potential gradient formed by the electron cooling
    - Ion beam acceleration along the plasma potential gradient
4) Interaction between the plasma current and the magnetic field during expansion
    - Diamagnetic current effect on axial plasma momentum
5) Plasma detachment from the magnetic flux line
    - Field stretching Breaking of adiabatic invariant, and various instabilities

As described above, the factors involved in ion acceleration in the magnetic nozzle are various [16-17]. In recent years, many topics have been discussed about the electric field formation by adiabatic expansion of plasma [18-25]. However, there is not much research based on the type of plasma heating. It is beneficial to classify different ion acceleration mechanisms depending on the origin of the internal energy used [52]. It can be divided into four general types of internal energy, depending on whether it is electron or ion energy and whether it is stored in the perpendicular or parallel direction. Each category for species and directions gives rise to a different mechanism: i) Parallel ion energy directly creates the gas dynamic acceleration or direct electro-thermal acceleration.

ii) Parallel electron energy is transferred directly into the ion energy through the ambipolar electric field, while generating part of the ambipolar acceleration. In addition, the electron population group is remarkably non-Maxwellian, it might give rise to local centralization of the ambipolar field, that could merge into non-neutral double layer [57]. The parallel energy mechanisms do not require interaction with the magnetic field and do not mean the gain of axial momentum. Indeed, the electric force which accelerates ions based on the ambipolar electric field and double layer mechanisms is inside to the plasma and merely converts electron to ion momentum, unless there is an externally applied electric field. Perpendicular energy, on the other hand, causes microscopic particle magnetic mirror acceleration, related to the gyro-motion of a charged particle in the magnetic field and the conservation of magnetic moment $\mu = mv_{\perp}^{2}/2\mathrm{B}$, which causes the perpendicular velocity to be converted for the parallel velocity in the direction of decreasing magnetic field intensities. iii) Perpendicular ion energy is converted to the axial energy, and iv) in the case of electrons, when the perpendicular energy is converted into the parallel energy, it is then used to accelerate ions via the ambipolar electric field as described above, accounting for the remainder of the ambipolar acceleration. Since the magnetic moment of the particles is opposed to the applied field, in both cases it is diamagnetic, and all acceleration due to mirror effect can also be called diamagnetic acceleration. In addition, in the presence of any particle drift perpendicular to the magnetic field, the interaction of the drift velocity with the external field generates a longitudinal force that can cause further acceleration depending on the drift motion direction. Note that in the case of perpendicular energy, the magnetic field is necessary for axial acceleration to occur, and the actual axial momentum gain is exerted on the propulsion system by the plasma-induced magnetic field generated by the combined magnetic moment of each the particles and their azimuthal drift velocities. Without structure of the magnetic nozzle, all perpendicular energy would instead be considered as losses as the non-confined plasma spreads radially.

1.2 Electron Thermodynamics in a Magnetically Expanding Plasma

As shown in the previous chapter, it is important to understand the process of electric field formation to achieve the ion acceleration efficiently. In particular, unlike ICH, which is a method of directly heating ions directly to increase the energy of ions [17], the acceleration of ions using purely electric field formed by magnetic nozzle type in low temperature plasma is efficient in terms of cost and maintenance. The electric field formation in a magnetically expanding plasma is associated with a variety of factors, and such issues are addressed in previous studies on magnetic nozzle.

Recently, the thermodynamic consideration of electrons has been revisited and applied to the ion acceleration in the magnetically expanding plasma [18]. The thermodynamic state of the plasma was understood using a polytropic index derived by the measured plasma parameters. Specifically, the adiabatic plasma expansion theory that induces ambipolar ion acceleration, which predicts the linear relationship between average electron energy and plasma potential, with the decrease of the average electron energy and the plasma potential, is presented. The electrons are assumed to be reheated to Maxwellian on a scale shorter than the electric field, resulting in Maxwellian distribution with temperature changes at all locations. The temperature then decreases with the possibility of balancing the electric and electronic pressures via the polytropic index. This is expressed as a polytropic equation, which suggests that the electron cooling rate and the plasma potential gradient are directly related to the polytropic index. However, this adiabatic expansion theory agrees with the adiabatic theory where the measured plasma potential and density correspond to an electron temperature and a degree of freedom of 3, which is inconsistent with the polytropic index from the relationship between electron temperature and plasma potential. There may be instability due to unknown density and magnetic field changes, or simply that the cooling of the entire electron is not operating in proportion to the potential change.

Since the revisited electron thermodynamics, it is recognized the electron heat conduction term in modeling for performance scaling of the magnetic nozzle devices [26]. The actual power emerging from the source exit is a function of the average energy lost per electron-ion pair ε leaving the source exit. The flow of the electron energy to the boundary of the source exit ε_{eff} can be estimated by the average energy loss per electron at the source exit expressed as the sum of enthalpy and heat flows as follows

$$\varepsilon_{eff} = \frac{3}{2}T_{\parallel,e0} + T_{\perp,e0} + \frac{mQ_e}{\dot{m}}, \tag{1.1}$$

where $T_{\parallel,e0}$ and $T_{\perp,e0}$ are the electron temperature in parallel and perpendicular direction to the paraxial magnetic field at the source exit, respectively, and Q_e is the electron power lost to magnetic field aligned heat conduction. Assuming that the potential energy along a magnetic field line is constant in the source region. Thus, the enthalpy consists only of thermal energy components $T_{e0} = T_{\parallel,e0} + 2T_{\perp,e0}$, taking into account the degree of freedom of electrons. The equation (1.1) indicates that the thermal energy and heat conduction of electrons determined at the boundary between the source and the expansion region directly contribute to the thermal conversion efficiency. Therefore, the importance of the determination of the electron thermodynamic properties has been emphasized in the modeling and experimental work conducted so far [27-31]. As an initial study [32] for evaluating magnetic nozzle performance, the magnetic field structure of the device was modified to a magnetic field configuration of de-Laval structure to generate supersonic plasma flow, and the experimental results were compared with the plasma 1-D modeling assuming isothermally behaving electrons with the Boltzmann relation ($Q_e = \infty$). In contrast, the adiabatic process assumption ($Q_e = 0$) with a slowly varying time dependent ambipolar electric field was considered for an analytical study of plasma dynamics in the expanding magnetic field [33-34]. Unlike the above studies, any determination of the electron power lost Q_e via the introduction of the polytropic index as a free parameter can promote the modeling tasks by providing the information about the plasma process. Similarly, in previous thruster models, the performance scaling on final exhaust velocity and the efficiency of detachment was analyzed along with equation of motion, where the polytropic index was treated as a free parameter derived from experimental values [18,26].

In summary, the previous studies have accomplished in simplifying the complex equation by introducing of the simple polytropic equation in theoretical and engineering aspects considering on the magnetically expanding plasma. The arbitrary chosen polytropic index as a free parameter for the determination of field-aligned heat conduction has contributed to undterstand various physical phenomena that have important implications in astrophysics and thruster modeling [60-64].

Since the study in the heat conduction term during effective internal energy loss, the new perspectives in the electron temperature term (i.e. thermal energy), have been increasing. Isothermally behaving electrons trapped in a potential well formed by a combination of an ambipolar electric potential and an external magnetic field exists together with adiabatically expanding electrons emitted from the nozzle throat [35-37]. The time-dependent kinetic properties of the magnetically expanding plasma as well as the time-resolved measurement of the EEPF were investigated [36]. The developed effective potential well leads to the trapping of the cooled electrons during the adiabatic expansion process and cut down the magnetic expansion region to the nozzle throat. As a result, the change in the EEPF revealed as the accumulation of the trapped electron group during adiabatic expansion causes a spatial change in γ that becomes closer to unity as it goes to the far-field region. To date, the non-adiabatic behavior is considered the presence of heat flux from the plasma source to the far-field region, so that the combination of the polytropic equation and the momentum conservation equation could determine an asymptotic value of the potential of the global diverging region. Unlike the previous studies on the topic of the heat transfer as a plasma source region, however, the study insists that the non-adiabatic behavior of an electron system is the main result of the trapped electron group generated in the local region separate from the source.

In addition to the above studies, the role of free electrons as wells the role of the trapped electrons is emphasized [39]. The specially constructed experiment shows the near perfect adiabatic expansion of an ideal electron gas resulting in a polytropic index greater than 1.4, approaching the adiabatic value of 5/3, when removing electric fields from the system, while the polytropic index close to unity is observed when the electrons are trapped by the electric fields. Keeping in mind the first law of thermodynamics, there must be no

heat transfer, but work must be done on the walls surrounding the system. Here, the expanding magnetic field can be considered as the wall that has work done on it, but as it is not a physical boundary, no heat is transferred. When the boundary sheath and ambipolar electric fields within the plasma are removed, none of the electrons are trapped in the plasma system and they, called free electrons, can only interact with the confining magnetic wall: the plasma pressure force does work on the magnetic boundary. In particular, a Lorentz force, created by inhomogeneities in the radial plasma density, does work on the expanding magnetic field, reducing the internal energy of the electron gas that behaves as an adiabatically expanding ideal gas.

1.3 Objectives and outline

The advantages of the magnetic nozzle concept are well known: wall-plasma contact is avoided, it provides a current-free plasma plume, it allows to control thrust by modifying the magnetic field geometry, etc. However, their industrial application requires the understanding of the physical mechanisms involved, such as the electron thermodynamics evolution at magnetically expanding plasma, which is crucial to determine propulsive performances. Since the introduction of the thermodynamics of electron in a magnetically expanding plasma, various phenomena are being discussed; the analysis from the heat conduction perspective, the formation of electric field by electrons trapped by magnetic moment, and the stretching of magnetic field and plasma detachment from the field by free electrons, etc. Regarding the plasma expansion, uncertainities arise under the collisionless regime, since in the absence of collisions, one is force to adopt electron temperature models to close the fluid equation hierarchy [40], but thus far, there is no evidence that an isothermal, adiabatic or polytropic law are theoretically well justified. For instance, an isothermal assumption is justifiable only if the distribution remains close to Maxwellian, which is not the case far downstream, since it leads to unbounded plasma acceleration and requires an infinite source of power. Moreover, adiabatic models cannot be justified in the collisionless regime, and a polytropic law requires an empirical justification. This motivated to study the plasma expansion with an electron thermodynamic description, in order to determine consistently the axial evolution of the electric potential and the electron energy distribution functions, and their associated properties such as the electron temperatures and electric potential drop.

The rearranging of the thermodynamically agreed consensus in previous studies is as follows. The entire system is called the electron gas, which is classified as an electron group trapped and escaping. The surroundings are called the electric and magnetic fields. The fields are flexible surroundings that can be changed by energy transfer. The energy of the system is reduced due to the adiabatic expansion of the free electron system and trapped electron system. From the point of view of total energy conservation, each the electron cooling lead to changes in the magnetic field and electric field. This implies that electron

confinement should be achieved for ion acceleration in low temperature plasma. Electron cooling by adiabatic expansion in the thermodynamic system is delivered to a certain object by the energy conservation in the whole system and do work to it. By the way, previous experiments and modeling studies have limitations in the understanding the phenomena assuming the isotropic expansion of plasma without considering the electron energy anisotropy. Therefore, a thermodynamic study of electrons that reflects the heating and energy exchange of each electron component is needed. Here, it extends to non-isotropic plasma with bi-Maxwellian electrons at the plasma reservoir with different temperatures in the parallel and perpendicular directions to the magnetic field, in order to study the effect of expanding an anisotropic plasma source through a magnetic nozzle. Indeed, this could be a case of especially interest for the ECR thrusters, since previous studies reveal that the electron temperature perpendicular to the magnetic field at the electron cyclotron resonance source is for instance higher than the parallel one.

The final goal of this study is to identify the mechanism of potential gradient formation in the magnetic nozzle considering the temperature anisotropy [41]. It also provides the insight into whether the field gradients for ion acceleration can be efficiently achieved. For the research on electron cooling and electric field formation based on the electron directional-selective heating mechanism of ECR source, the changes in electron energy distribution function (EEDF) of each directional component of electron via ECR power are diagnosed. Ultimately, study on the correlation between the thermodynamic state of each temperature component and the plasma potential gradient will be shown.

This thesis is organized in the following order: After the introduction, the experiment setup and diagnostics are described in Chapter 2. This chapter introduces the magnetic nozzle device with an ECR plasma source and electrostatic Langmuir probes for anisotropic plasma diagnostics. Also, the collisionless plasma conditions to be satisfied for the reliability of polytropic equation and probe measurements are presented. In Chapter 3, the magnetic nozzle plasma parameters will be characterized in paraxial region with a cylindrical Langmuir probe. And thermodynamic analysis of electrons via EEDF shows that there are spatially different plasmas in terms of polytropic index, which are related to electron cooling and variation of potential. The transition in the thermodynamic properties

in magnetically expanding plasma is confirmed by the derived effective polytropic index. In Chapter 4, the measurement results using independent directional Langmuir probe considering the heating characteristics of the plasma source are shown. The selective heating to the perpendicular to the magnetic field creates a unique anisotropic energy distribution dissipation. Next, the correlation between anisotropic electron thermodynamics behavior and total potential build-up is analyzed by applying the total energy equation in terms of the energy cooling and transfer of each the trapped and escaping electron group in Chapter 5. Finally, in Chapter 6, the overall conclusion and future work are represented.

Chapter 2 Experimental Setup and Diagnostics

2.1 Magnetic Nozzle

2.1.1 Magnetic Nozzle with ECR Plasma Source

As shown in Fig. 2.1, the linear plasma device for magnetic nozzle consists of the driver region including a typical electron cyclotron resonance (ECR) plasma source operating at 2.45 GHz wave frequency and the diffusion region where a cylindrical chamber is surrounded by a pair of solenoid coils for generating various curved magnetic field structures [42]. Two different regions are separated by a magnetic nozzle depicted as NF coil. Hence, high density plasmas generated by ECR heating in the driver region is transported into the diffusion region through the magnetic nozzle. The ECR plasma is chosen as a plasma source due to its ability of effective heating in low pressure and high degree of ionization. Magnetic nozzle experiments are carried out in the diffusion region where various magnetic field configurations can be produced by a pair of solenoid coils. A vacuum pumping system consists of a 350 L/min oil sealed rotary pump and a 1,000 L/sec turbo molecular pump. The working gas is injected through a gas feeding port by a mass flow controller with a maximum flow-rate of 50 mL/min. The base pressure is ~7×10^{-7} Torr and the typical operating pressure the order of 10^{-4} Torr. The main parameters of the magnetic nozzle device system are listed in Table 2.1. In the driver region, the magnetic field of 875 G (resonant magnetic field for 2.45 GHz) is produced by two identical solenoid coils named ECR field (EF1 and EF2) coils axially placed on the cylindrical vacuum chamber. The maximum 1.5 kW RF power is injected in parallel to the magnetic field from a 2.45 GHz magneton (ASTEX, FI20061) source through a WR284 waveguide. During the power delivery, the impedance between the source and the load is automatically matched by an auto-matching system (ASTEX, SmartMatch^{TM}). The end of the waveguide is placed between the EF1 coil and the EF2 coil for high field side launch (HFS) to avoid the cut-off for the right hand circularly polarized wave (R-wave).

Additional nozzle field (NF) coil is installed at the right end of the driver chamber to form converging diverging magnetic field configuration since it allows to convert thermal energy of ions to their kinetic energy. In the diffusion region, two guiding field (GF1 and GF2) coils are arranged outside the diffusion chamber. These coils can make various magnetic field configurations such as parallel beam, cusp, or gradually diverging magnetic fields depending on the amplitude and polarity of GF coil currents. In this work, the GF coils are not used. A cylindrical Langmuir probe (CLP), a directional Langmuir probe (DLP) and a triple Langmuir probe (TLP) array are installed in the diffusion chamber for measuring plasma properties of diffused plasmas, respectively. The probes are located at the position on the z-axis. All of the electrostatic probes can be moved along z-direction (3 cm - 57 cm) by linear feedthroughs.

Magnetic field structure produced by the electromagnets can be calculated with a 2-D magnetic field solver based on the Green's function. In Fig. 2.2, the strength of Bz along the z-axis of the device is plotted to identify the position of ECR layers. The optimum magnetic field configuration is found in the case of the combination (I_{EF1} = 60 A, I_{EF2} = 60 A, and I_{NF} = 200 A), because the ECR layer is so close to the diffusion chamber that the particle density of the exhausted plasma may be higher. The absorption of microwave (MW) power is calculated using an AC/DC and a RF module built in COMSOL Multiphysics® software. The intense absorption of MW power occurs near the expected position of the ECR layer.

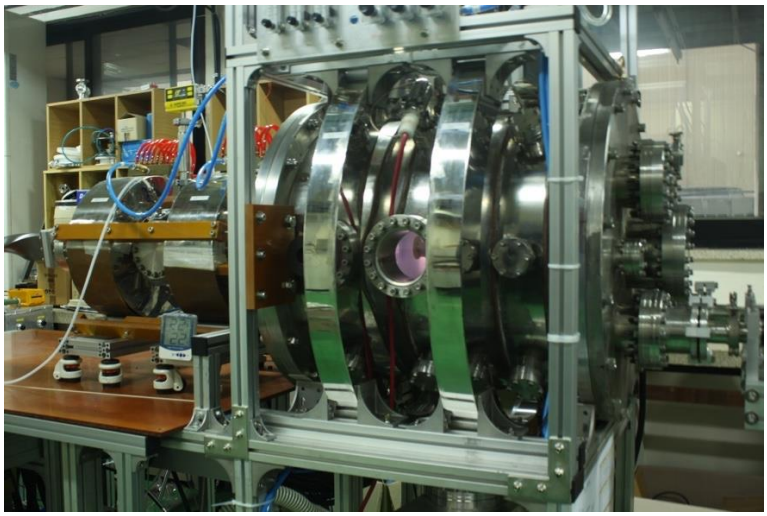

(a)

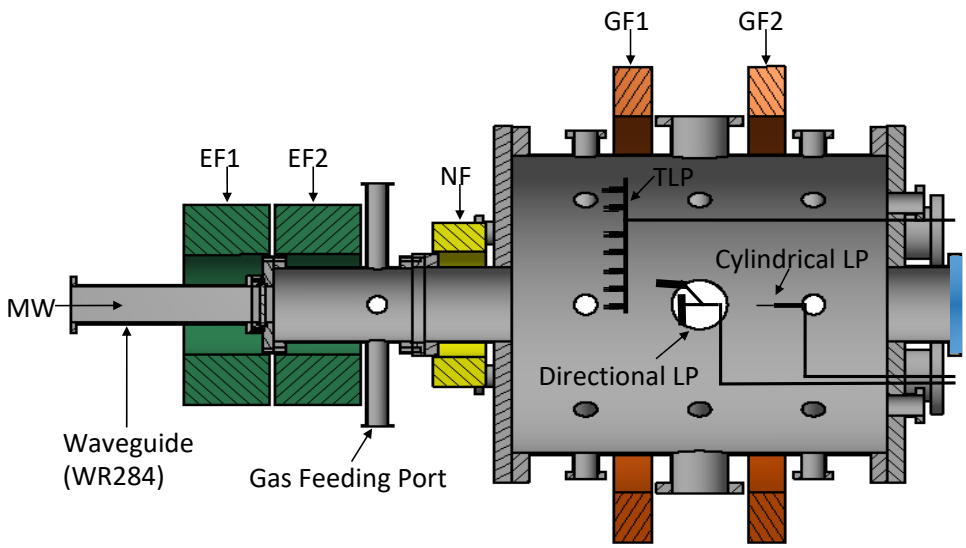

(b)

Figure 2.1 (a) Photograph of the magnetic nozzle device with ECR. (b) Cross-sectional view of the magnetic nozzle showing the ECR plasma source region and diffusion region with axially movable directional Langmuir probe (DLP), cylindrical Langmuir probe (CLP) and triple Langmuir probe (TLP) array.

Table 2.1 Operational conditions of the magnetic nozzle device.

Gas	He, Ar	Frequency	2.45 GHz
Base pressure	$7.0X10^{-7}$ Torr	EF coils	60 A
Operating pressure	0.15 - 0.9 mTorr	NF coil	0 - 200 A
MW power	200 – 1200 W	GF coils	-50 - 50 A

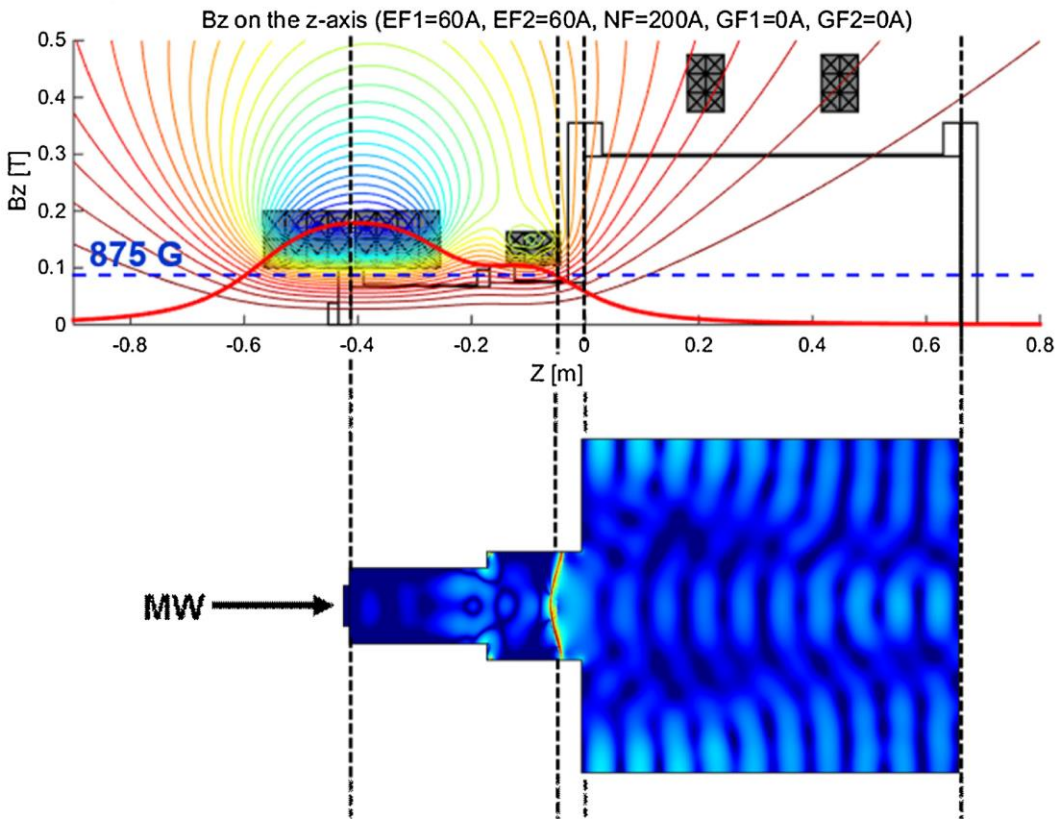

Figure 2.2 Magnetic field configuration and electron cyclotron resonance layer. (top) Contour plot on the magnetic flux and profile of field intensity (thick line) on z-axis. (bottom) Distribution of absorbed power calculated by COMSOL program package.

2.1.2 Collisionless Plasma Condition

The reason why thermodynamic properties should be understood in the low temperature plasma of the magnetic nozzle in the laboratory environment is that ion acceleration can be achieved by the inter-electron energy transfer and the electron cooling, and thus the formation of the electric potential gradient. In order to achieve the purpose of this study, the following three conditions must be satisfied. Firstly, the plasma characteristics are diagnosed using a planar Langmuir probe in the magnetized plasma, where the collision of electrons in the sheath region of the probe electrode must be ignored. Second, the polytropic equation should be fulfilled in the magnetic nozzle plasma. This indicates that no electrons and ions should be produced when expanding. Third, the electric field must be generated by the electron cooling. For this result, the thermal equilibrium must not be maintained. All of the above conditions are possible only if the plasma is in a collisionless regime.

This chapter describes the major assumptions for collisionless plasma, based on the calculated plasma parameters shown in Table 2.2. The calculated parameters are defined under assuming that 0.1 eV of the Argon ion temperature and the low and high magnetic field condition with microwave power of 600 W corresponds to 0 A and 200 A of NF coil current, respectively. Since the ionization degree defined as the ratio of the electron to neutral particle number densities is below 0.15%, the long-range Coulomb collisions including electron-electron and electron-ion collisions can be neglected for weakly ionized plasmas. Rather, the collision process is dominated by short-range collisions between charged electron and neutral. At the operating pressure (Argon 0.4 mTorr) ensures nearly collisionless plasma expansion; the mean free path for electron-neutral collision (110 cm) is much longer than chamber length (66 cm) in expansion region.

Table 2.2 Collisionless plasma condition at the nozzle throat in low and high magnetic field by NF coil.

Parameters at nozzle throat (z = 3 cm)	Low magnetic field (I_{NF}=0A)	High magnetic field (I_{NF}=200A)
Ionization degree [%]	0.15	0.07
Magnetic field [G]	110	490
Electron temperature [eV]	6.5	9.3
Electron density [X 10^{10} cm^{-3}]	2.6	1.1
Electron Larmor radius [cm]	0.06	0.04
Ion Larmor radius [cm]	1.5	0.7
Electron mean free path [m]	1.1	1.1

2.2 Plasma diagnostics

2.2.1 Cylindrical Langmuir probe

The Langmuir probe would be the most popular tool to diagnose low temperature plasma because of its simplicity and high spatial resolution [43]. What we have to do is to plasma a small conducting tip in plasma and measure currents as varying voltages on it. From the correlation between the measured current and voltage, plasma properties can be analyzed. Single tip Langmuir probe, most widely used among the probes, gives basic properties of plasmas such as electron temperature plasma density, plasma potential and floating potential, and electron energy distribution function. Compared to the data acquisition with the probe, theories to get plasma properties from the current-voltage data are more complicated and should be selected carefully, considering plasma conditions such as collisionless or collisional, magnetized or unmagnetized, high or low density, and so on.

A cylindrical probe tip is made of a tungsten (W) wire whose diameter is 0.3 mm and length is 4 mm in this experiment. Debye length of the magnetic nozzle plasma is typically ~0.1 mm. Thus, the charge particle collecting area of the probe can be assumed as same with the probe tip area. In order to analyze I-V curve of the Langmuir probe, the collisionless sheath model is applied. The cylindrical Langmuir probe measurement was conducted on the paraxial region of the diffusion chamber. The probe can be moved from the nozzle throat (z=0 cm), to the far-field (z = 52 cm). The diagnostic was conducted at every 2 cm along axis. To obtain I-V curve with low noise, the probe current was averaged of 200 cycles of the probe voltage sweeping.

The process of producing EEDF from the I-V curve, which is the result of the probe measurement, involves second derivative method, commonly called the Druyvesteyn method, and first derivative method used in the bi-Maxwellian distribution. In the case of the cylindrical probe measurement, second derivative method was used because there is little difference in the results of two methods. Generally known, as the EEDF progresses to higher energy the electron current to the probe gets smaller and the second derivative is more prone to noise. At higher energy the resolution is increased to reduce the noise. The

second derivative of the IV characteristic is related to the EEDF by the Druyvesteyn equation [43]:

$$\mathrm{n}(\varepsilon) = n_e f(\varepsilon) = \frac{2I''}{eA_p}\left(\frac{2m\varepsilon}{e}\right)^{\frac{1}{2}}, \tag{2.1}$$

where I'' is the second derivative of the I-V characteristic, and ε is the energy given by (V_p-V). Note that the second derivative displayed in uses 3 points derivative smoothing technique. The second derivative used for the EEDF calculation uses a single point method to preserve all the features of the EEDF.

Following several plasma parameters can be derived from the EEDF. The electron density is calculated by numerical integration (using the trapezoidal method) of n(ε),

$$\mathrm{n}_e = \int_0^{\varepsilon_{max}} \mathrm{n}(\varepsilon)\, d\varepsilon. \tag{2.2}$$

The average electron energy is calculated using:

$$\langle\varepsilon\rangle = \int_0^{\varepsilon_{max}} \varepsilon f(\varepsilon)\, d\varepsilon. \tag{2.3}$$

The electron temperature for a Maxwellian EEPF is defined as

$$kT_e = \frac{2}{3}\langle\varepsilon\rangle. \tag{2.4}$$

This relationship is used to calculate the electron temperature from the EEDF for all EEDF types. When the EEDF is non-Maxwellian the result is often called the effective electron temperature kT_{eff}.

2.2.2 Directional Langmuir probe

A directional Langmuir probe (DLP) [44-45] which consists of two-independent molybdenum planar-type electrode and alumina insulator tube was used. Fig. 2.3 show a feature of a fabricated planar type directional Langmuir probe. Each probe electrodes were constructed from molybdenum of 5.5 mm in diameter. Since the planar probe head have longer radius than the electron Larmor radius (0.04 mm), the electrons run to the probe tips as an infinite plane. Around the edges of the electrodes tips are covered with a liquefied insulator. This is to reduce the electric field effect caused by sheath expansion occurring around the edge of the electrode. The insulator and electrode are connected carefully so as to maintain an interspace gap between them and prevent an increase in surface area that could happen as a result of electrode sputtering. The two electrodes are fixed so as to be approximate 90 degrees in order to measure the parallel direction and the perpendicular direction of the magnetic field, respectively. However, the vertical electrode, which measures the electron movement in the perpendicular direction, has a very small amount of electrons that strike it actually, when it is completely parallel to the magnetic field. This can cause difficulty in drawing the I-V curve by probe measurement, so the electrode is tilted by approximately 5 degrees to fix toward the plasma.

Each the probe current-voltage characteristics measured in perpendicular and parallel direction is shown in Fig. 2.4. It has been reported that with a grazing incidence of the magnetic field to the probe electrode, electron current I_e and ion current I_i decrease and V_f increases, and these features are also observed in the present results. In the near-nozzle region, the ion current in the parallel direction is larger than the ion current in the perpendicular direction due to the characteristics of the directional Langmuir probe measured in each direction with respect to the magnetic field. In the far-field region under the isotropic condition, there is almost no difference in the ion current part.

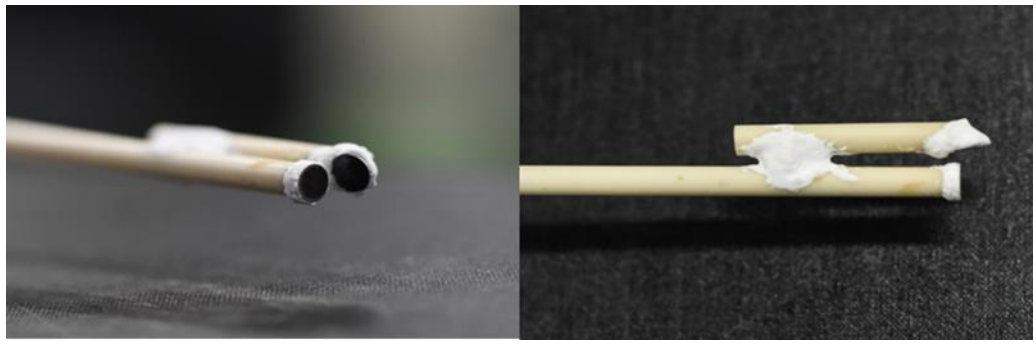

(a)

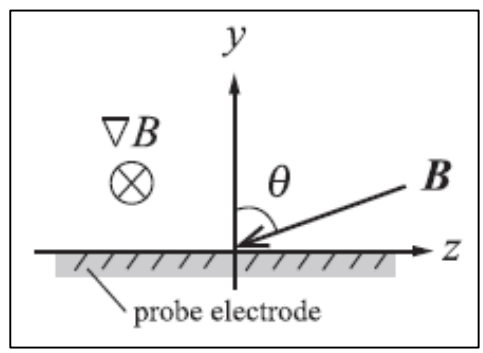

(b)

Figure 2.3 (a) Photograph of a fabricated planar type Directional Langmuir probe; two planar Molybdenum tips are placed in a nearly vertical direction. (b) A coordinate system used for the electron trajectory [45].

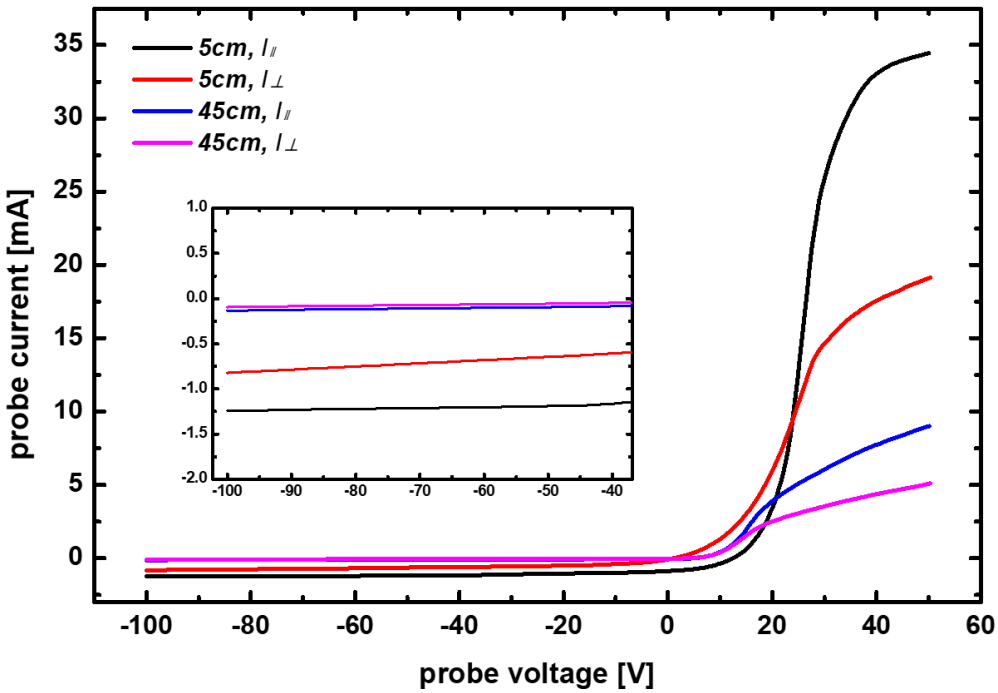

Figure 2.4 Typical I-V curve characteristics of planar-type directional Langmuir probe.

2.2.3 Measurement of Electric Energy Distribution Functions

Anisotropy in the EEDF in an ECR plasma with weakly magnetized ions and magnetized electrons is experimentally investigated using a directional Langmuir probe. Under an assumption of independent EEDFs in the directions parallel and perpendicular to the magnetic field, the directional variation of the EEDF can be evaluated. In a magnetized plasma, a reduction in the cross-field particle flux results in the elongation of the electron and ion collection volumes along the magnetic field. In this case, an attachment of the opposite side of the collection volume to the other surfaces or an extension of the volume to longer than the characteristic spatial scale of the plasma parameters could cause significant errors in the interpretation of the probe current-voltage characteristics. Furthermore, the EEDF pertaining to the parallel and cross-field flux components maybe different because of the difference in their collisionalities. However, from practical point of view, it has been reported that T_e and n_e evaluated by using the unmagnetized probe theory empirically agree with other methods to within a factor of 2, where T_e is the electron temperature, and in particular when the probe biasing voltage is below the floating potential, the error becomes smaller. As an alternative approach, a kinetic model that describes electron collection using a diffusion approximation has been proposed for a plasma in which only the electron is magnetized. The model is well arranged in reference [45].

As discussed about the cylindrical Langmuir probe, in general, the Druyvesteyn method, which integrates the second derivative of the I-V curve in the entire energy region and obtains the electron density, is a method widely used in the probe theory for the plasma measurement. It is used regardless of the probe geometry assuming the isotropic EEDF. However, if the degree of anisotropy of the plasma is large (i.e. high magnetic field or different energy heating state for the perpendicular and parallel direction), the Druyvesteyn method cannot be used. The method of obtaining the EEDF by first derivative should be used [46-47]. To improve a consistency of the I-V curve analysis and reduce a time to analyze the I-V curve, a Impedans ALP System^{TM} control unit is introduced as shown in Fig. 2.5.

From I-V curve, floating potential, plasma potential, electron temperature and electron density are defined as followings. The floating potential V_f is the potential developed at a surface in contact with a plasma when electrically isolated from ground. Since there is no net current flow the potential develops such that the electron and ion fluxes are equal. On the I-V characteristic the probe potential that collects zero net current is equivalent to the plasma floating potential. The plasma potential V_p is the point on the characteristic in the electron retardation region when the collected electron current departs from an exponential and enters the electron saturation region. In this region the probe current increases more slowly. The first derivative of the I-V characteristic will show a peak at the transition between the two regions. The probe voltage at which this peak occurs is used to calculate the plasma potential. A robust method for calculating the electron temperature kT_e is used, compared to finding the slope of the region between V_f and V_p. The current at the plasma potential $I(V_p)$ is divided by the integral of the characteristic between V_f and V_p as following:

$$\frac{1}{kT_e} = \frac{I(V_p)}{\int_{V_f}^{V_p} I_e(V)\, dv}. \tag{2.5}$$

And the probe current measured at the plasma potential $I(V_p)$ is used to calculate the electron in the plasma:

$$n_e = \frac{I(V_p)}{A_p}\sqrt{\frac{2\pi m_e}{e^2 kT_e}}, \tag{2.6}$$

where A_p is the probe area, m_e is the electron mass, and e is the electron charge.

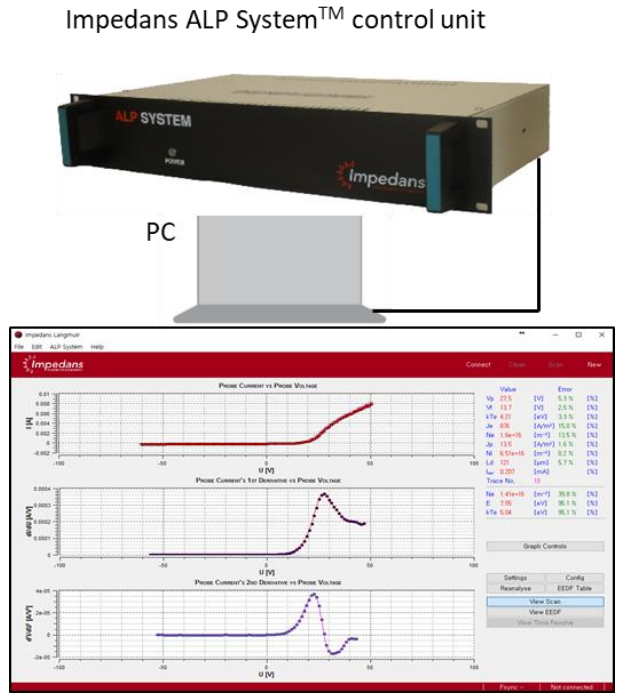

Figure 2.5 Data acquisition system (DAQ) including Impedans ALP System™ control unit and its typical display panel on the i-v curve.

Chapter 3 Characterization of Magnetic Nozzle Plasma

3.1 Paraxial Measurement of Plasma Parameters

Experiments on plasma potential build-up for ion acceleration in a magnetic nozzle were performed in the magnetic nozzle device, a linear plasma device with ECR plasma source. The diagrams of the magnetic nozzle configuration are shown in Fig. 3.1. The measurements were conducted in argon plasmas with two magnetic field conditions of high field (nozzle coil on) and low field (nozzle coil off), respectively. The mass flow rate is 4 sccm, and the operating pressure is 3×10^{-4} Torr. Microwave with a frequency of 2.45 GHz and a power of maximum 1.2 kW was then fed into the vacuum chamber for hours. The plasma is initiated on the ECR layer, which has a spheroid shape, and the magnetic field strength on the surface is 875 G. The field direction can be reversed by switching the polarity of the current. The cylindrical-type Langmuir probe was installed on the mid-plane of the device outside the ECR layer at diffusion region, where the r-z coordinate system is defined, and the origin of the coordinate system is located at the center of the device. At the position of the probe head, the magnetic field strength was approximately from 500 G to 100 G along the distance, z, and the field direction was nearly perpendicular to the probe axis.

Axial profiles of the parameters were measured between 3 and 52 cm downstream of the magnetic nozzle throat. These values are shown in Fig. 3.2 for mass flow rates of 4 sccm and ECR power of 600 W. The scope of errors in the plasma density, potential, and electron temperature were ±15%, ±0.5V, and ±0.5 eV, respectively, over the whole range of axial positions. The plasma density, potential, and electron temperature all decayed as the magnetic field strength decreased downstream of the throat of the magnetic nozzle. Especially in the case of a high magnetic field, the electron temperature is observed to drop sharply depending on the space. The significant temperature gradient is called the electron cooling. That is the plasma thermodynamic state is not isothermal in this case. For each

magnetic field condition, the absolute value of the plasma potential is different, but the total potential drop seems to be similar.

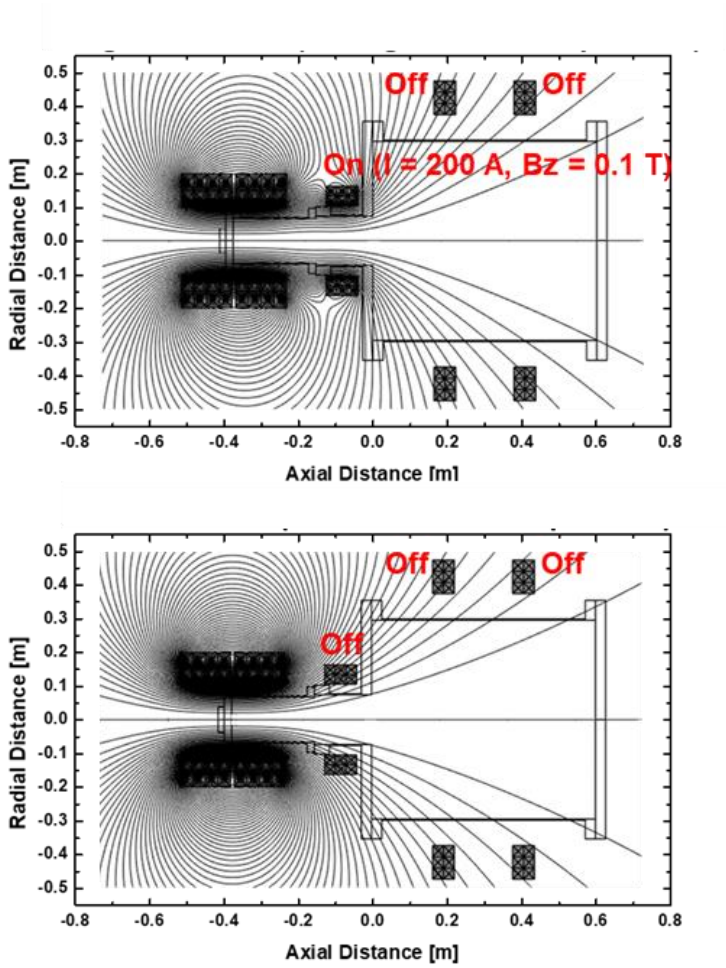

Figure 3.1 (top) A schematic diagram of magnetic nozzle field configuration with NF coil current on, and (bottom) NF coil current off.

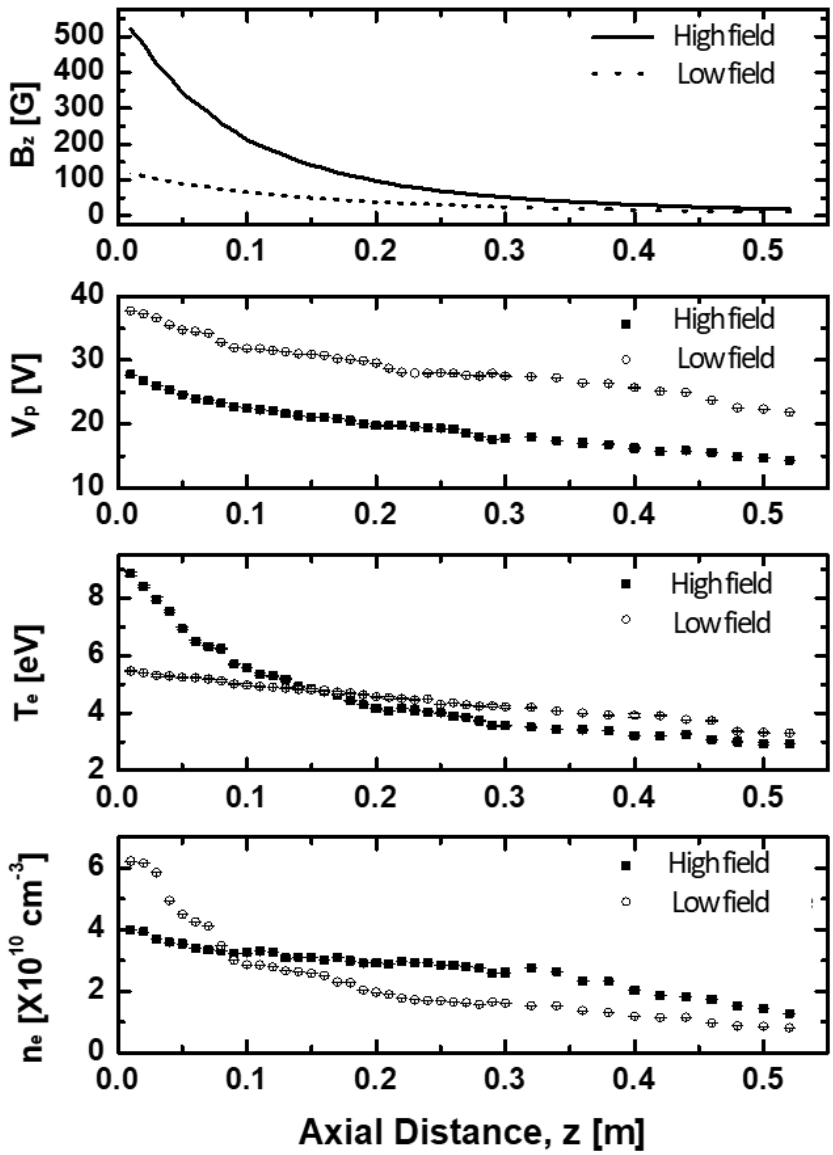

Figure 3.2 Axial profiles of plasma parameters measured by cylindrical-type single Langmuir probe from 3 cm to 52 cm from the nozzle throat at 200 A for high field (close square), and 0A for low field (open circle): axial magnetic field strength B_z, plasma potential V_p, electron temperature T_e, and electron density n_e as a function of distance.

3.2 Electron Thermodynamic Perspective in Magnetically Expanding Plasma

The previous studies have succeeded in simplifying the energy equation by introducing of the polytropic equation in the magnetically expanding plasma. Using the identical methodology, the polytropic index can be driven. The index represents the electron thermodynamic characters in the magnetic nozzle. From the momentum conservation equation,

$$\rho\left(\frac{\partial}{\partial t}+\boldsymbol{v}\cdot\nabla\right)\boldsymbol{v}=-\nabla\cdot\boldsymbol{P}+\rho\boldsymbol{E}+\boldsymbol{j}\times\boldsymbol{B}+\rho\boldsymbol{g}+\boldsymbol{R}\ , \tag{3.1}$$

where the ρ is number density, $\boldsymbol{v}$ is drift velocity, $\boldsymbol{P}$ is pressure, $\boldsymbol{E}$ is electric field, $\boldsymbol{j}$ is current density, $\boldsymbol{B}$ magnetic field intensity, $\boldsymbol{g}$ is gravitational acceleration constant, and $\boldsymbol{R}$ is term for the other forces such as radiation loss. In condition of steady state, gravity force and radiation loss is negligible. The reduced the electron momentum conservation equation is as follows

$$\frac{\partial p_e}{\partial s}=n_e\frac{\partial(e\phi)}{\partial s}\ , \tag{3.2}$$

where p_e is electron pressure, s is unit direction vector along the magnetic flux and ϕ is electric potential. Assuming that the magnetized plasma does not exchange the energy with their surroundings. Introducing the following equation of state for adiabatic plasma,

$$P\cong P_e=Cn_e^{\gamma}\ , \tag{3.3}$$

where $\gamma=(N+2)/N,\ p_e=n_eT_e$, the relation among the electron temperature, electron density and plasma potential can be simplified. C is coefficient constant, γ is polytropic index, and N is degree of freedom. From the equation (3.1) and (3.2), three simple relations are derived as follows

$$\frac{\partial(e\phi)}{\partial s} = \frac{C\gamma}{\gamma - 1}\frac{\partial\left(n_e^{\gamma-1}\right)}{\partial s} \ , \tag{3.4}$$

$$\frac{\partial(e\phi)}{\partial s} = \frac{\gamma}{\gamma - 1}\frac{\partial T_e}{\partial s} \ , \tag{3.5}$$

$$\frac{\partial T_e}{\partial s} = C\frac{\partial n_e^{\gamma-1}}{\partial s} \ . \tag{3.6}$$

The relation between electron temperature and plasma potential in the above equations implies that the loss of average electron energy contributes to the formation of the plasma potential via polytropic index. The local electron thermodynamic characteristics play an important role in determining the macroscopic ion acceleration.

Using the simplified equations, each the constant polytropic index is deduced by the linear regressions on two stages as shown Fig. 3.3. Double polytropic indexes are experimentally drawn in an adiabatic expansion of the magnetic nozzle. The thermodynamic characteristics are clearly different depending on the case of each magnetic field state. When the nozzle is formed with a high magnetic field, it has two polytropic indices. The downstream side is a thermodynamic state with an isothermal-limit state at 1.17, which is close to 1. On the other hand, if the magnetic field is relatively low diffusion, it is always isothermally spatially maintained. There is non-equilibrium of electrons in the plasma expansion.

From the measured axial variation of EEDFs obtained at 10 cm intervals from 1 cm (near-nozzle) to 50 cm (far-field) from the nozzle throat at two nozzle types ($I_{NF} = 200\ A$ and $0\ A$) as shown in Figure 3.4, spatial evolution of EEDFs can be distinguished in each case. At high field in Figure. 3.4(a), the magnitude of the electron density observed in the low electron energy region along the axial direction does not largely change, but it can be seen that electrons are spatially cooled from the high energy electron depletion. This means a significant cooling of high energy electrons in a strongly magnetized plasma electrons. On the other hand, at low field in Figure 3.4(b), it is observed that the electron density varies greatly in the low electron energy region along the axial direction and almost no

electron cooling occurs in the high electron energy region. From the results in the two magnetic field conditions, it is driven when the effect of the nozzle is strengthened, the electron cooling is enlarged, and then the adiabatic expansion and, conversely, isothermal expansion when the nozzle effect is weakened.

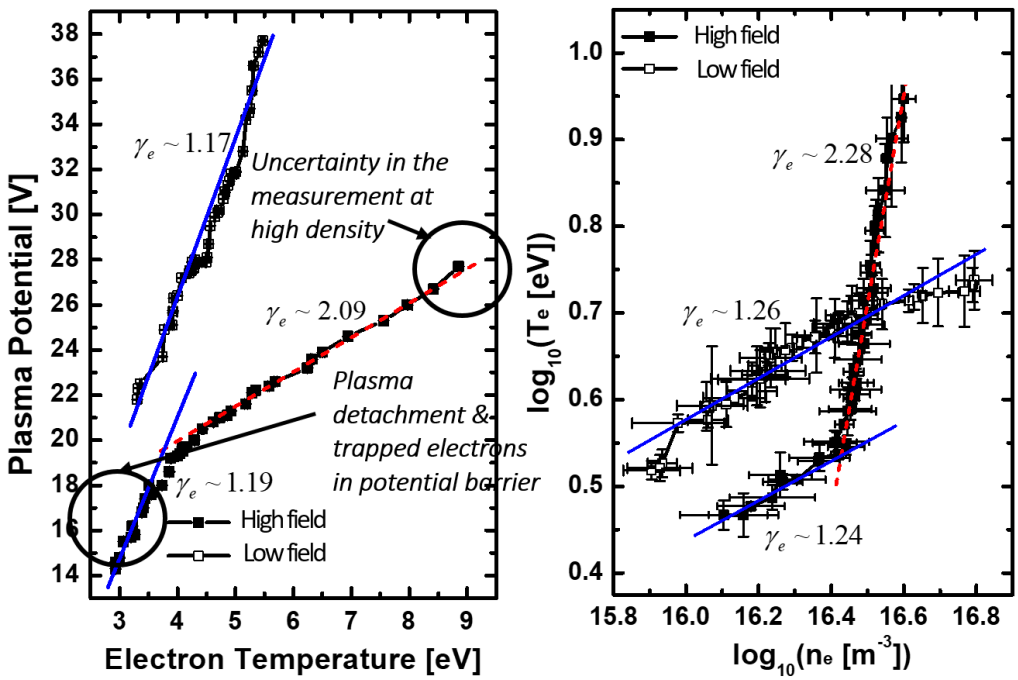

Figure 3.3 (left) Linear relationship between electron temperature and plasma density for high magnetic field (close square) and low magnetic field (open square), and (right) Log-scaled linear relationship between electron density and electron temperature for high magnetic field (close square) and low magnetic field (open square).

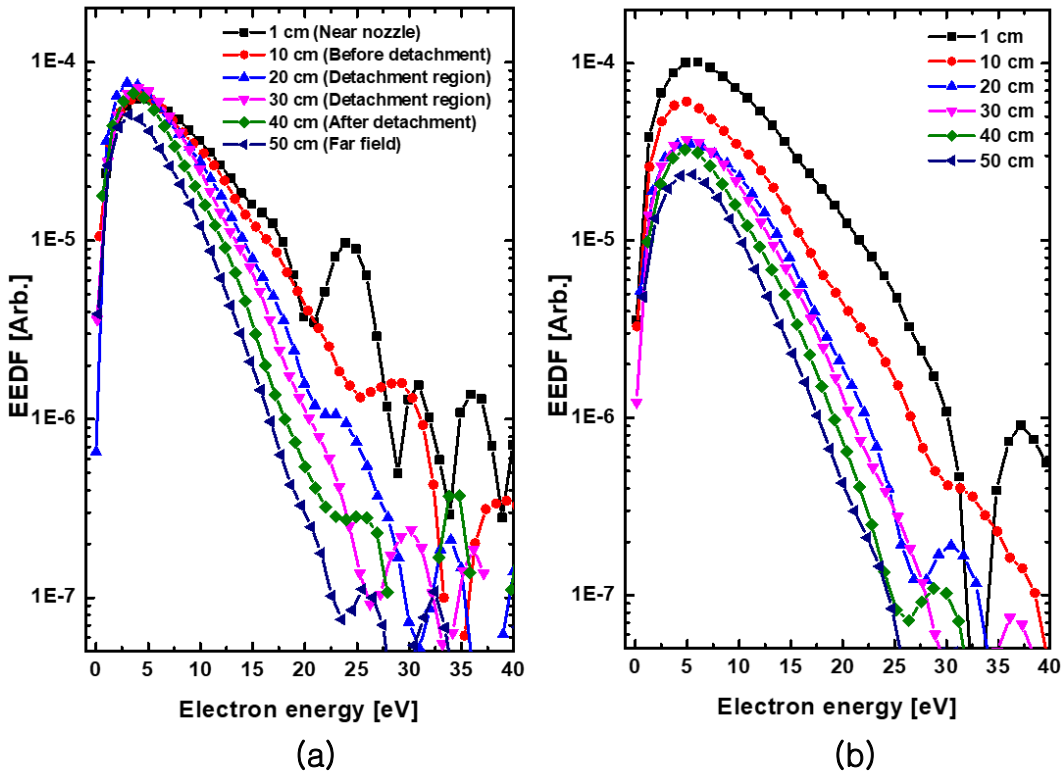

Figure 3.4 Axial variation of EEDFs in electron energy measured in (a) high field configuration, and (b) low field configuration at 10 cm intervals from 1 cm (near-nozzle) to 50 cm (far-field).

3.3 Thermodynamic Phase Transition in Adiabatic Expansion of Magnetized Plasma

The polytropic index, which is know from the experimental results, can be plotted along the axial distance. The value of the data point at each position of the rate of change of the plasma parameters is difficult to be spatially drawn because it is difficult to be continuously differentiated. So each the spatial profile estimated the gamma value, that is the polytropic index from discontinuous points by maximally smoothing at a level where there is little loss of shape. Figure 3.5 shows the spatial variations of the electron polytropic index, γ_e from the plasma parameters.

We find that the correlations along the axial streamline exhibit two well-defined power laws, which is represented to polytropic equation, suggesting that there are three distinctive regions in magnetically expanding plasma. The first region ($\gamma_e \sim 2 \pm 0.15$) approximately coincides with the beam core region. The high value more than typical polytropic index, 5/3 for ideal monatomic gas. This is 2-D adiabatic compression when the polytropic index is 2. Another simple approach is to set the value to 2 because the degree of freedom is 2 in a magnetized plasma in the 2-D plane. In the region, the electrons exhibit significant cooling as they are emitted out from the source. Previously, it was established that the electrons are trapped by the potential well in the adiabatic expansion and become thermalized. As a result, the electrons reach a new equilibrium. The second region (decreases γ_e) is the transition region from adiabatic state to isothermal-limit state. In the region, electrons also exhibit significant cooling. The plasma expansion in the region is non-equilibrium. In the thermodynamic phase transition region (z ~ 10 – 30 cm), there are several factors that can cause the instabilities such as trapped electron in potential barrier, turbulence due to space charge effect, and cross-field diffusion. In the third region ($\gamma_e \sim 1.17 \pm 0.03$), effective electron temperature is constant. This is because the electric field in the region is small and there are no significant energy loss mechanisms for the collisionless electrons.

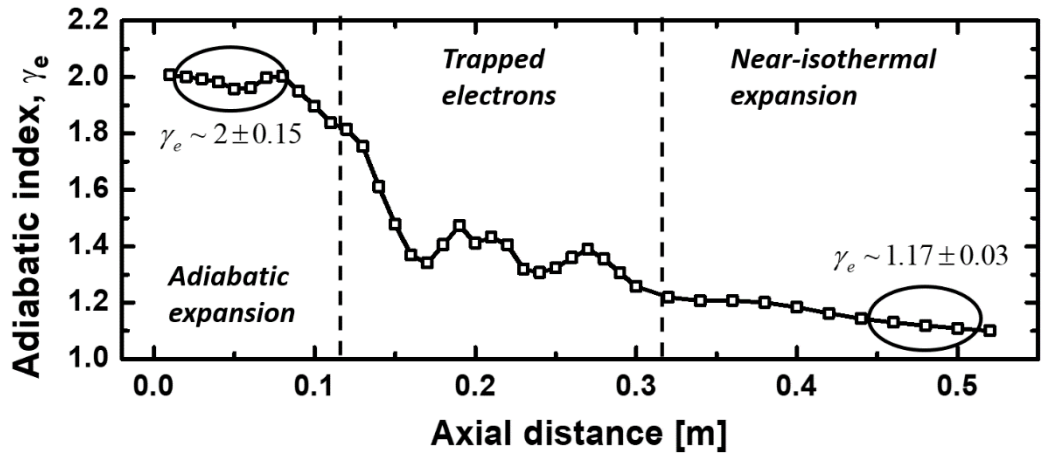

Figure 3.5 Spatial variations of the electron polytropic index, γ_e from the adiabatic equation of state.

Chapter 4 Anisotropic Electron Thermodynamic Analysis with Direction-Independent Measurement

In the previous chapter, overall plasma characteristics were obtained by using cylindrical Langmuir probe in magnetically expanding plasma. The thermodynamic properties of the magnetic nozzle were investigated using the polytropic index obtained by measuring the effective electron temperature and the plasma potential. We found the interesting result of the transition in the polytropic index in the adiabatic expansion process along the magnetic field. This phenomenon has also been observed in the results from particle simulations [40,53]. In addition, the measurement of the plasma flow in different directions at the front and back plate using a double-sided planar Langmuir probe is similar to the change in the overall thermodynamic properties due to the trapped electrons [48]. However, in previous studies, including the results of our group [38, 42, 48] has been studied the thermodynamic characteristics assuming that the energy of the plasma source is isotropy without considering the directionality of electron energy in both experiment and modeling. Considering the anisotropy of the electron temperature can be important in forming the electric field which determines the efficiency of the ion acceleration effect of the magnetic nozzle [41].

4.1 Anisotropic Electron Energy Distribution Functions with Directional-Selective Heating

Before observing changes in spatially anisotropic plasma, it is investigated the anisotropy [58, 59] of the local plasma in the nozzle throat region near the ECR plasma source. Note that assuming the plasma generated in the source region is transmitted along the uniform magnetic field line to the nozzle throat. The change in the plasma source characteristics as the MW power increases is invariably moved to the change of plasma parameters in the nozzle throat (z = 5 cm).

As shown in Fig. 4.1, it is observed that each the aspect of electron heating measured by the DLP in perpendicular and parallel direction differs according to the MW power. At low MW power, the parallel electron energy distribution is clearly shown bi-Maxwellian distribution. As the plasma source power increases, the electrons in the parallel direction become Maxwellized as the electron-electron collision. It can be seen from the slope of the EEDF. On the other hand, in the perpendicular electron energy, the EEDF in high energy region is depleted, and as the power of the plasma source increases, the slope of the EEDF decreases, which means that the high energy electron region in the perpendicular direction is being heated. In other words, it implies that the effective electron temperature in the perpendicular direction is increasing. This is due to the selective heating of the perpendicular electrons of the ECR plasma source, which is the result of the natural source characteristics that resonate with the frequency of electron gyromotion in the magnetic field.

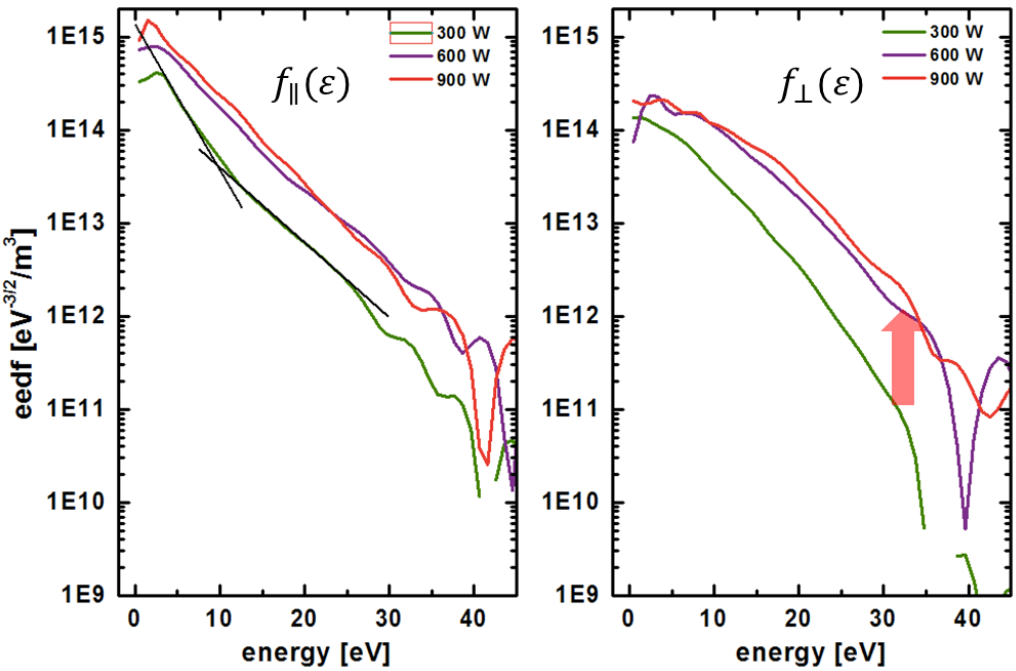

Figure 4.1 Heating of electrons in both the directions according to MW power. (left) Maxwellianization of eedf in parallel direction due to increased electron-electron collision, (right) Heating of high energy electron region in perpendicular direction with directional-selective heating.

4.2 Spatial Evolutions of Plasma Parameters

Figure 4.2 shows the axial profiles of plasma parameters measured by planar-type DLP from 3 cm to 57 cm from the nozzle throat at NF coil current of 200 A for high field in perpendicular direction and in parallel direction, respectively. Under an assumption of independent electron energies in the parallel and perpendicular directions to the magnetic field, each the directional electron temperature and density, and plasma potential are evaluated. All of the plasma parameters are spatially decayed, but they show a much greater reduction in the perpendicular electron energy when is separated independently in each direction. In particular, the higher the power, the higher the perpendicular electron temperature near the nozzle throat region, resulting in significant electron cooling in the phase space. On the other hand, the parallel electron temperature is hardly cooled from the nozzle throat region, then there is almost no difference in the entire space.

The plasma potential is measured independently in the perpendicular and parallel direction, but the value of the plasma potential measured from the perpendicular probe is used. The plasma potential should be a non-directional scalar value. Ideally, each the plasma potential in the perpendicular and parallel direction is identical, but there is a slight difference, approximately 1-2 V, in the plasma potentials measured in the two directions, depending on the experimental limitations in which the same position cannot be measured accurately. As well as the plasma potential obtained through the perpendicular probe is used for the result analysis in order to avoid the influence of the distortion of the electron saturation current region on the I-V curve caused by the ion beam component on the plasma potential. In the case of the electric thruster, there is an ion beam with the high directional energy. When measuring with a planar probe in the direction of corresponding with the beam direction the ions are reflected in front of the plate, and the generation of this region produces large sheath and electron currents. In the I-V curve, there is possibility of distortion in the vicinity of the plasma potential [47]. As a result, when the ion beam with directional energy exists in the anisotropic plasma such as the thruster, the anisotropic property causes a drifting distribution and distorts the plasma potential. Therefore, using the perpendicular direction probe data is reliable. On the premise of the above, the plasma

potential is decaying, but there is no significant difference in the potential gradient even when the MW power is increased. Rather similarly, the potential gradients are produced, with the trend of decreasing gradients in the far-field region. Finally, the logical proposition, based on the previous studies that increases the electron temperature increases the formation of the potential gradient is reversed from this experiment result. Rather, increasing the MW power caused a decrease in the plasma potential gradient in the far-field region. We need a clear physical understanding of this result for efficient ion acceleration effect in the magnetic nozzle. A detailed analysis is presented in Chapter 5.

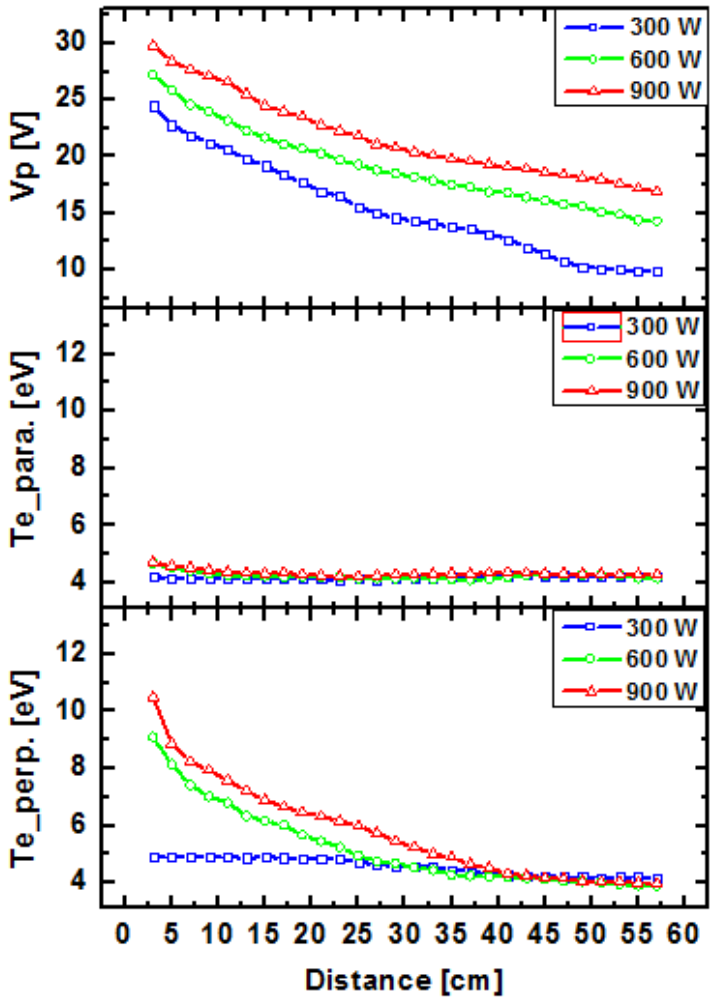

Figure 4.2 Axial profiles of plasma parameters measured by planar directional Langmuir probe from 3 cm to 57 cm from the nozzle throat at 200 A for high magnetic field; plasma potential V_p, parallel electron temperature $T_{e,para}$. and perpendicular electron temperature $T_{e,perp.}$ as a function of distance.

4.3 Anisotropic Electron Energy Dissipation

Under an assumption of independent EEDFs in the directions parallel and perpendicular to the magnetic field, the directional variation of the EEDF is evaluated. The EEDFs is measured from the probe current-voltage characteristics with the aid of first derivative method taking into account the parallel and perpendicular motions of the electrons. Each the axial variations of EEDF with low and high power are obtained as shown in Fig. 4.3 and Fig 4.4. The distinctive difference of EEDF between the two conditions of low and high MW power is observed in the low electron energy region of the parallel electron distribution and the high electron energy region of the perpendicular electron distribution. High energy depletion from the perpendicular EEDF and the change to low in slope in the parallel EEDF of 5-15 eV energy range occur simultaneously as the plasma expands spatially.

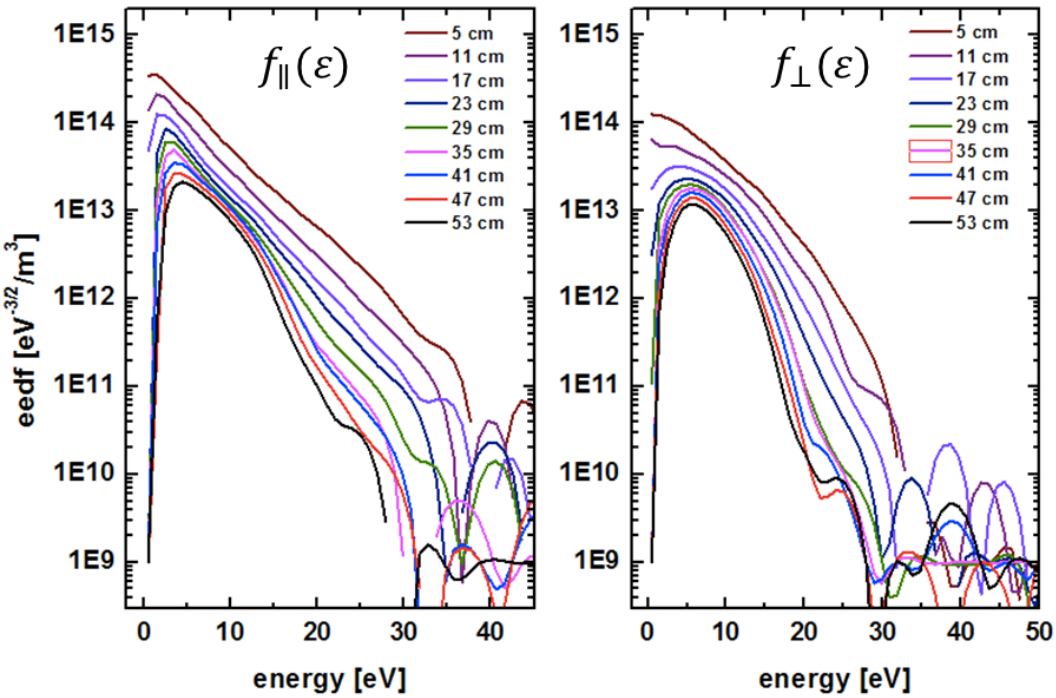

Figure 4.3 Axial variation of EEDFs measured in the parallel direction (left), and perpendicular direction (right) from 5 cm (near-nozzle) to 53 cm (far-field) with low MW power (300 W).

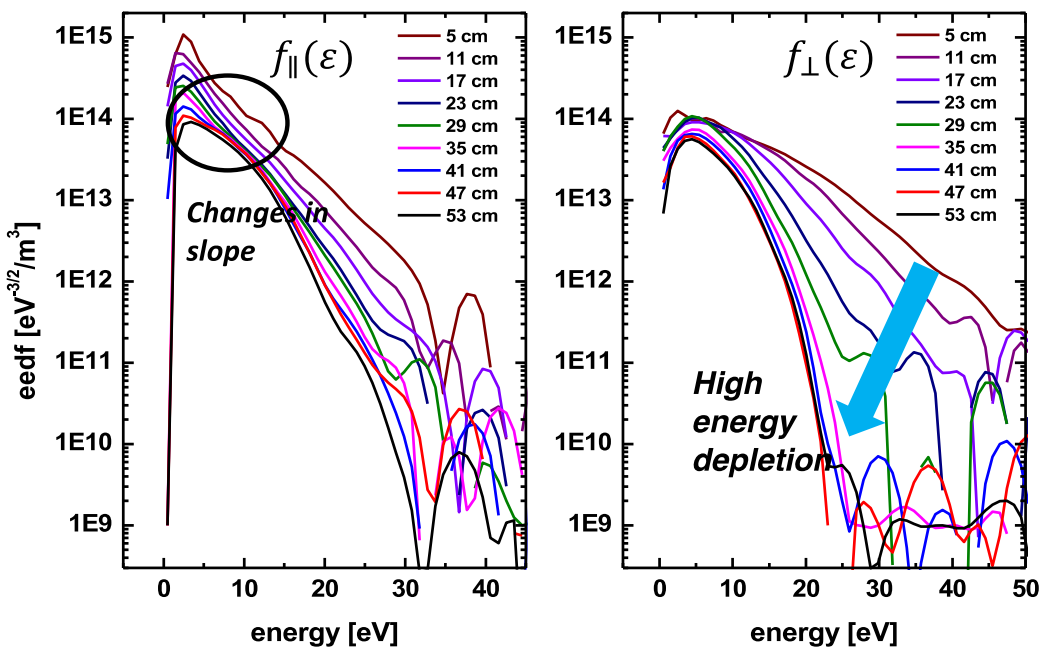

Figure 4.4 Axial variation of EEDFs measured in the parallel direction (left), and perpendicular direction (right) from 5 cm (near-nozzle) to 53 cm (far-field) with high MW power (600 W).

Fig. 4.5 is shown that the difference in the degree of energy cooling of the electrons in the independent direction becomes clearer along the spatial variation. This behavior is related to the conversion of radial and azimuthal energy of the free electron subpopulation into axial energy due to the diverging electric potential and the conservation of perpendicular pressure. The electron cooling is dominated by electron energy distribution in the perpendicular direction.

The degree of the cooling differs by independently thermodynamic behavior in each direction, which can also be confirmed by the polytropic index. From the relation of plasma potential and electron temperature, the polytropic index is calculated independently for each direction. The relationship between the electron temperature and the plasma potential analyzed earlier is also applied in this section. The relationship between the rate of change of the electron temperature in independent directions and the plasma potential can be explained by the polytropic index. The process is shown in the following Fig. 4.6(a). It can be seen that each slope is in a different independent state.

In the same way, a spatial profile for an independent polytropic index for each direction can be drawn in Fig. 4.6(b). There are different thermodynamic properties of electrons in each direction, because of the anisotropic nature of electron in ECR plasma. Free electrons have parallel polytropic index < 5/3 (under adiabatic) and perpendicular polytropic index > 5/3 (over adiabatic) in a near-nozzle region. From an effective polytropic index [65] for the electron, which is arranged in terms of the temperature anisotropy and the gradient of flow velocity, it can be expected to be higher value than 5/3 for an ideal gas as shown in Appendix I. The effective polytropic index consists the internal energy ε and volume expansion rate $K = \nabla \cdot \boldsymbol{u}$ as follows

$$\gamma_{eff} = 1 + \frac{1 + \dfrac{2\varepsilon_{\parallel} K_{\parallel}}{\varepsilon_{\perp} K_{\perp}}}{\left(1 + \dfrac{\varepsilon_{\parallel}}{\varepsilon_{\perp}}\right)\left(1 + \dfrac{K_{\parallel}}{K_{\perp}}\right)} = 1 + \frac{1 + 2\alpha\beta}{(1+\alpha)(1+\beta)}, \tag{4.1}$$

where the α is temperature anisotropy and β is expansion anisotropy. The anisotropic electron energy distribution due to ECR is related to the effective polytropic index and plasma potential. Ion acceleration can be determined with this factor. Fig. 4.7 is shown the correlation with effective polytropic index and internal energy anisotropy.

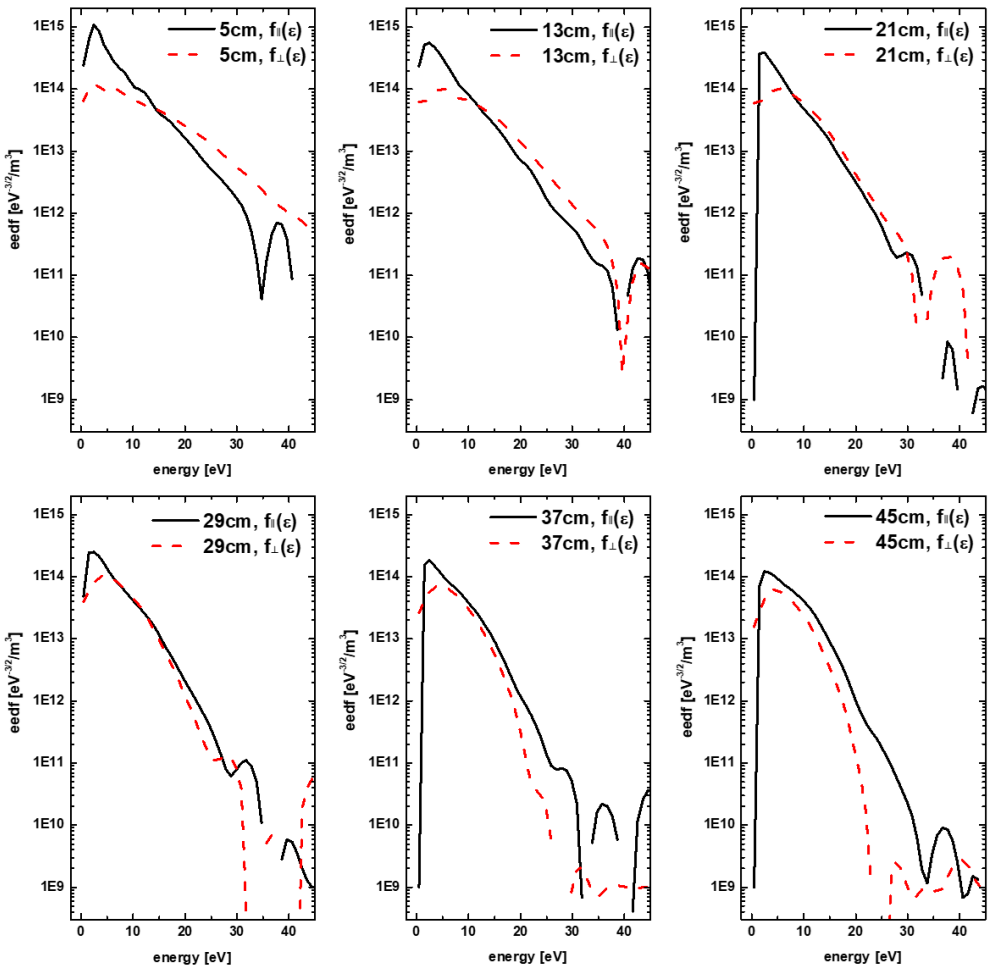

Figure 4.5 Spatial thermodynamic behavior compared with perpendicular and parallel distributions in a local position.

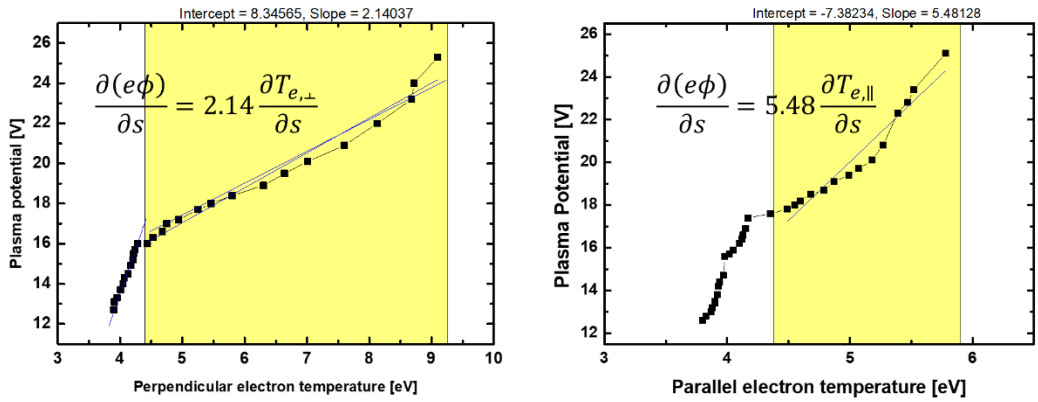

(a)

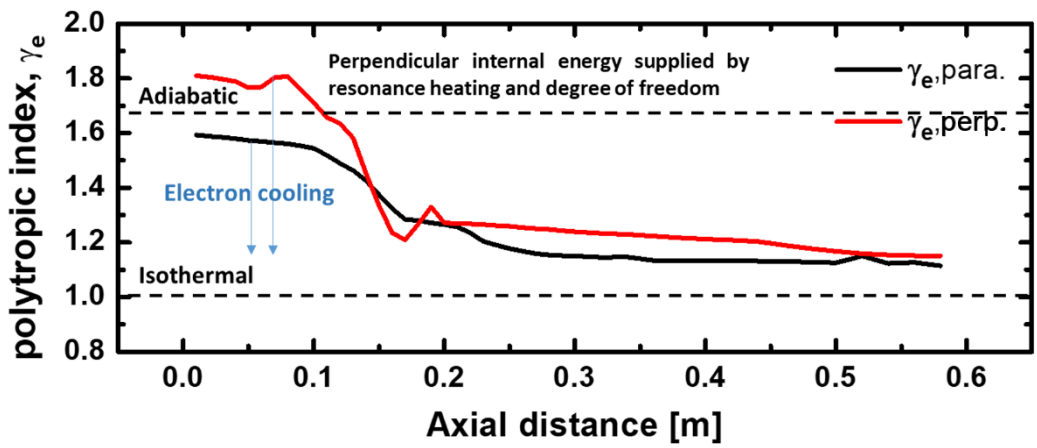

(b)

Figure 4.6 (a) Linear regression method from the plasma potential and electron temperature independent on the direction for deduction of the polytropic index, and (b) Spatial profile of the polytropic index independent on the direction.

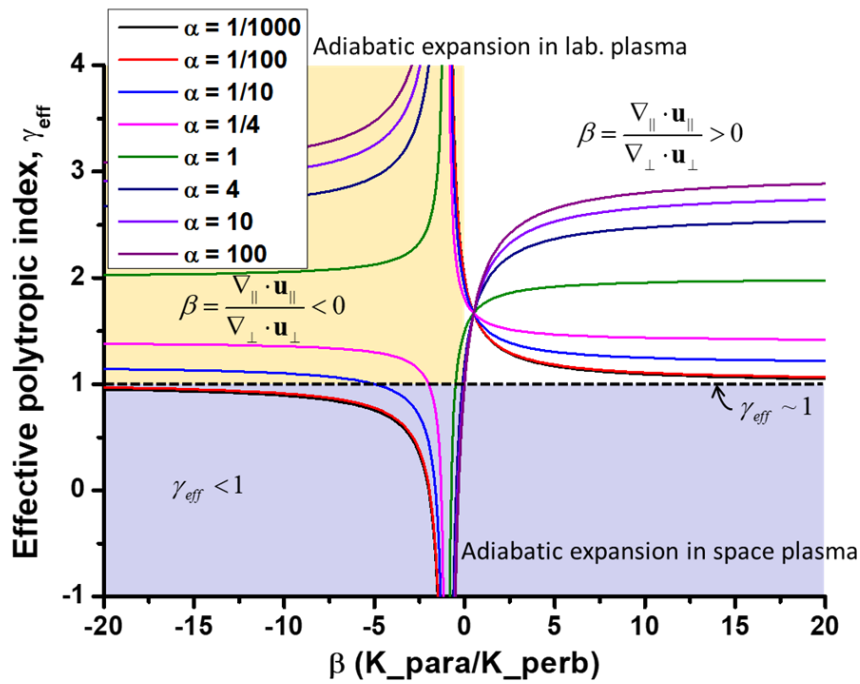

Figure 4.7 Effective polytropic index including temperature anisotropy and volume expansion anisotropy.

Chapter 5 Correlation between Anisotropic Electron Thermodynamic Behavior and Electric Potential Build-up

We observed that the distribution of high electron energy region is increased by selective heating in the perpendicular direction with increasing microwave power in Chapter 4. The heated perpendicular electron energy is cooled along the expanding nozzle magnetic field, while the parallel electron energy is hardly cooled. At this time, the difference in potential gradient according to the power resulted in not much difference. From the spatial variation of EEDF, we obtained an unusual phenomenon in which the energy depletion of the perpendicular electrons in the high energy region and the uplift of the slope of the parallel electron energy distribution in the low energy region. This chapter refines the thermodynamic behavior of electrons with anisotropic properties based on the observed EEDF properties. An insight in the correlation between the energy transfer by energy conservation of electron groups with different properties and the potential gradient formation is presented.

5.1 Methodology for the Definition of Trapped and Escaping Electrons

Previous studies on the thermodynamic behavior of electrons in magnetic nozzles have focused on groups of the bouncing electrons confined by magnetic fields and escaping free electron groups. Electrons having total electron energy, $E_{e,T}$ higher than the total potential drop, $|e\phi_\infty|$ can move freely toward the chamber wall, while it remains confined to electrons bounce back and forth within the maximum magnetic moment well, if the total electron energy is lower than the total potential drop. The local maximum magnetic moment with total energy can be expressed as follows: $\mu_{e,m} = (E_{e,T} + e\Delta V_p)/B_z$, where V_p is the plasma potential and B_z is axial magnetic field intensity. The state of each electron group was defined as "Free" or "Escaping" and "Trapped" or "Confined" [39, 49,50].

In this study, from the analysis of EEDF, these electron groups are distinguished by the electric potential barrier. As shown in Fig. 5.1, the area where the total electron energy distribution is smaller based on the plasma potential is the trapped electron group ($E_{e,T} < V_p$)and the area where the distribution is larger than the plasma potential is defined as the escaping electron group ($E_{e,T} > V_p$). The plasma potential is then based on the value of the electrostatic potential measured by the electrostatic probe. In other words, the low energy electrons that cannot escape the electric field are trapped, and the electrons of higher energy than the potential energy of the electric field escape the electric field and run toward the chamber wall.

Fig. 5.2 shows the arranged thermodynamic classification of the anisotropic electron energy in the magnetic nozzle plasma. The electrons are trapped or escaping to/from the electric field depending on their energy distribution. Each the trapped electron group and the escaping electron group can be distinguished as having internal energy that is perpendicular and parallel to the magnetic field.

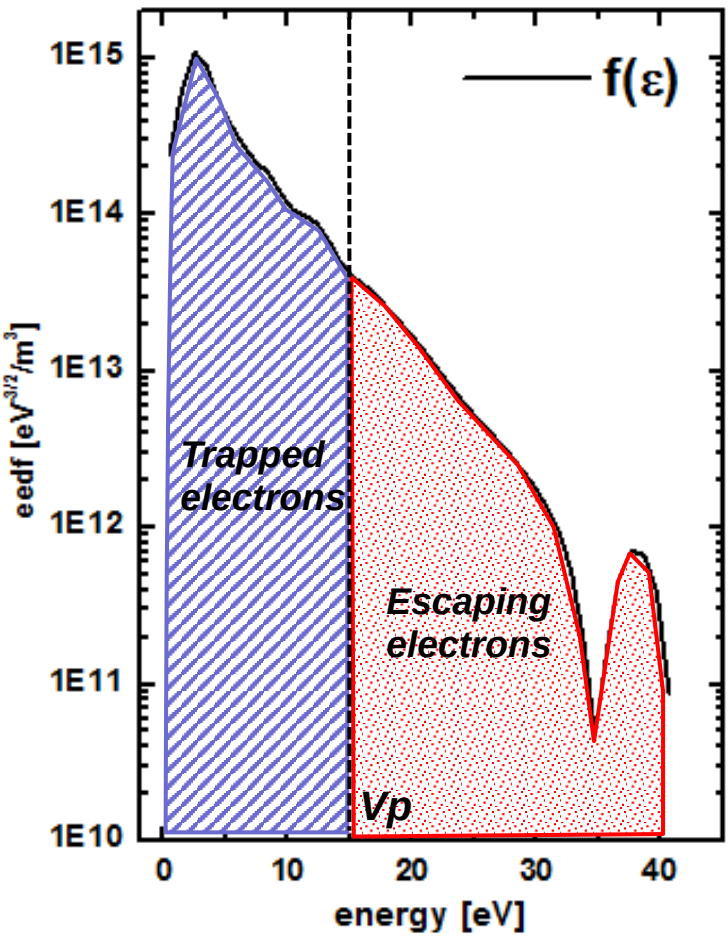

Figure 5.1 Determination of the trapped and escaping electron group.

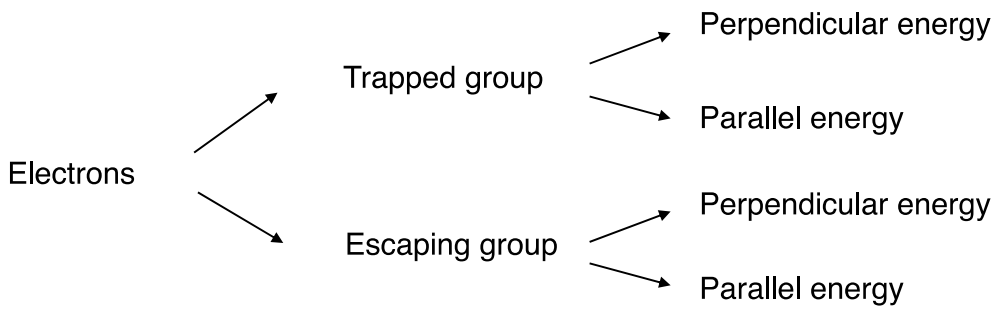

Figure 5.2 Category of anisotropic thermodynamic group in magnetic nozzle.

5.2 Electron Cooing and Energy Transfer in Total Energy Conservation Perspective

In order to understand the energy transfer in the cooling and heating of the electron energy from interpreting the EEDF, an approach from the point of view of the total energy conservation law is needed [39]. The total electron energy is expressed as the sum of the thermal kinetic energy and the potential energy in the independent perpendicular and parallel directions:

$$E_{e,T} = \frac{1}{2} m_e \left(v_{\parallel,e}^2 + v_{\perp,e}^2 \right) + e\phi. \tag{5.1}$$

Since the electrons in the adiabatic expansion are not exchanged between the system and outside, it means that the energy exchange between thermal kinetic energy and the potential energy in each direction may be possible. If the magnetic moment is conserved in the diverging magnetic field, the adiabatic invariant of an electron is expressed in the relation to the perpendicular electron velocity and the magnetic field as follows,

$$\mu_e = \frac{m_e v_{\perp,e}^2}{2B}. \tag{5.2}$$

This means that the perpendicular electron energy decreases as well in the magnetically expanding plasma under the assumption which the magnetic moment is conserved.

In order to explain the thermodynamic energy transfer of electrons in this experiment, we need to verify that this invariant is valid. Basically, the condition that the magnetic moment of gyrating particles is not maintained can be classified as follows: 1) High collision frequency, 2) Oscillation in the frequency due to high cyclotron heating, and 3) Cyclotron frequency is less than the change in the magnetic field (i.e. magnetic cusp with almost no magnetic field). Applying the above conditions to the experimental environment, the magnetic nozzle plasma has a collisionless where the mean free path is longer than the chamber size. Also, the nozzle magnetic field does not change abruptly as the cusp magnetic field. Thermodynamically, the electrons are cooled as much as the magnetic field

decreases along the space, so that they tend to be constrained to move by the magnetic field line. In fact, it can be quantitatively confirmed that the region where the magnetic moment of electrons is broken does not exist in the magnetic nozzle chamber.

It deals with demagnetization of the particles with non-uniform magnetic moment, via a relation of Larmor radius, ion velocity, magnetic field strength, and scale length of magnetic field inhomogeneity in terms of a single particle. The conservation of magnetic moment of a particle is broken if

$$\kappa \frac{dB}{dt} > B f_{c,\alpha} \tag{5.3}$$

is satisfied. In the equation, $f_{c,\alpha}$ is the electron or ion frequency, κ is a correction factor. The derivative of magnetic field with respect to time can be expressed by the gradient of space in z-direction as

$$\kappa v_{z,\alpha} \nabla_z B > B f_{c,\alpha} \ , \tag{5.4}$$

where v_z is the flow velocity in the z-direction. From the above equation, the following inequality condition is derived for the particle detachment:

$$\xi = \left| \frac{f_{c,\alpha} L_B}{v_\alpha} \right| = \left| \frac{qB}{m_\alpha v_\alpha} \right| \left| \frac{\nabla B}{B} \right|^{-1} < \kappa \ , \tag{5.5}$$

where ξ is the non-adiabaticity parameter [42, 51, 54] for the electron and ion species, L_B is the characteristic scale length of the magnetic field inhomogeneity, q is the electric charge, and m is the mass, respectively. Consequently, the non-adiabaticity parameter has a physical meaning which is a degree of particle detachment from magnetic field estimated by comparing the transport time of the field gradient experienced by the motion of the particle to the cyclotron frequency. The non-adiabaticity parameter is calculated using Eq. (5.5). It is assumed that Te is as the measurement value, Ti = 0.1Te, and v is the thermal velocity. The calculation result is shown in Fig. 5.3. Since the correction factor κ is order unity [51], in the case of ions, a region with a small scale length of the inhomogeneity of

the field experienced by the movement of ions with respect to the ion cyclotron period may exist in the chamber, thereby separating the ions from the magnetic field. In the case of electrons, this parameter is very large order of 10^2, and at least in the diffusion chamber, the magnetic moment is difficult to break, which makes it difficult for electrons to escape from the magnetic field.

As a result, the electrons are strongly magnetized in the chamber scale and the magnetic moment is conserved. This suggests that the energy can be transferred to the electrons and potential in the parallel direction due to the energy cooling in the perpendicular direction in terms of total energy conservation.

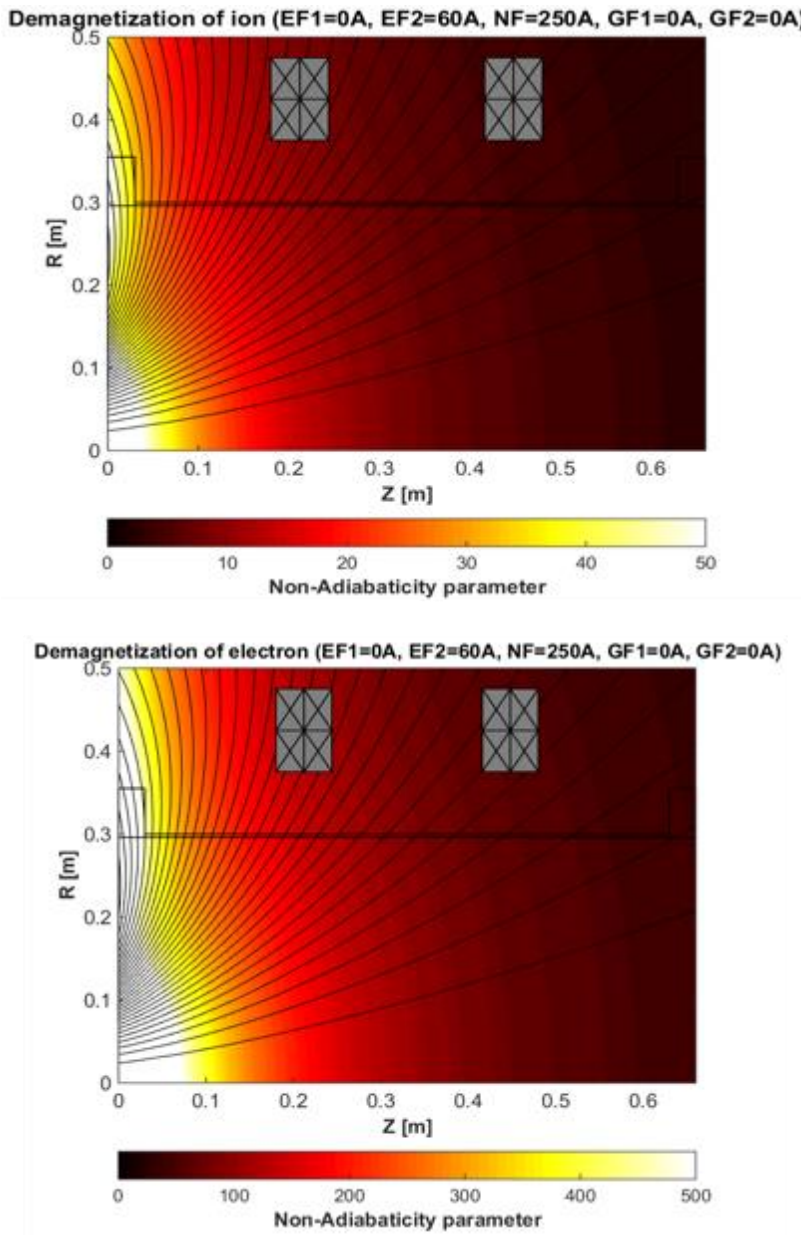

Figure 5.3 Contour map of the non-adiabaticity parameter in the expanding plasma for the demagnetization.

The plasma potential also varies with spatial variation in the EEDF for each direction measured independently from the DLP. In order to simplify the characteristics of the electron group based on one potential reference, the plasma potential measured at the point closest to the nozzle throat was selected to shift the EEDF at different positions by the potential difference to make the total energy equal. From this method, the trapped electrons group and the escaping electron group can be easily observed for each location based on the identical plasma potential.

The magnetically expanding plasma exhibits a large change in properties at approximately z = 30 cm from the experimental measurements in this study. This can be confirmed from the change in profile of the spatial polytropic index and the change and the plasma potential gradient. Therefore, we analyze the energy transfer by dividing the space into near-nozzle region (Region 1) and far-field region (Region 2). In addition, the case of low power (300 W) and high power (600 W) is compared to investigate how the difference in the electron energy increase in a specific direction due to the wave heating is caused by the cooling by the space.

The EEDF is shown in Fig. 5.4 for the spatial variation of low and high power in region 1. When the electron heating is small, there is only a slight change in the slope of the energy distribution of the electrons in the perpendicular direction, and as a whole, the slope of the EEDF does not change significantly with the space. Despite the vicinity of the nozzle throat, the degree of the electron heating is low, then the cooling does not occur significantly. On the other hand, when the electron heating is relatively more done, it can be observed that the energy gradient of the electron in the perpendicular direction changes rapidly from low slope side to the high slope side. This can already be seen in the perpendicular electron temperature profile. This means that the cooling of the electrons in the high energy region (i.e. the escaping electron group) is dominant. On the other hand, the electron energy in the parallel direction seems to have only a slight cooling without significant change in the space. The EEDF results in region 1 are somewhat contrary to expectations in terms of total energy conservation that the perpendicular temperature rises due to the increased ECR power will transfer the energy to the parallel electron and the plasma potential. Since the significant cooling the escaping electrons does not make a large

difference in the potential gradient, it can be estimated that the escaping electron group is not involved in the potential formation and is working on other uncertain surroundings.

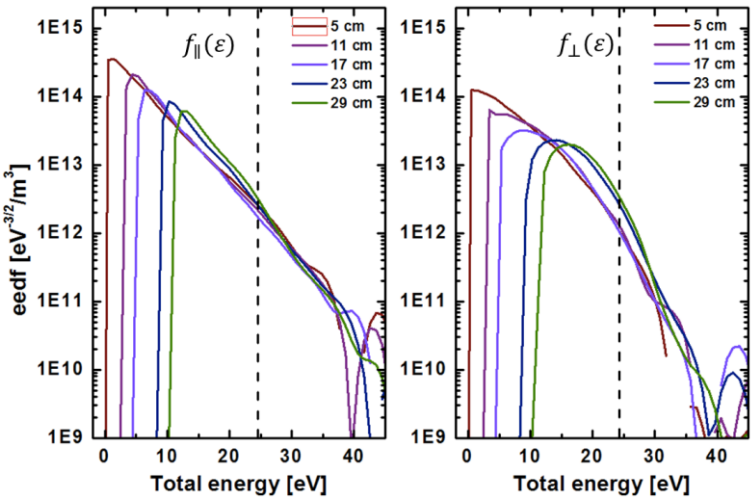

(a)

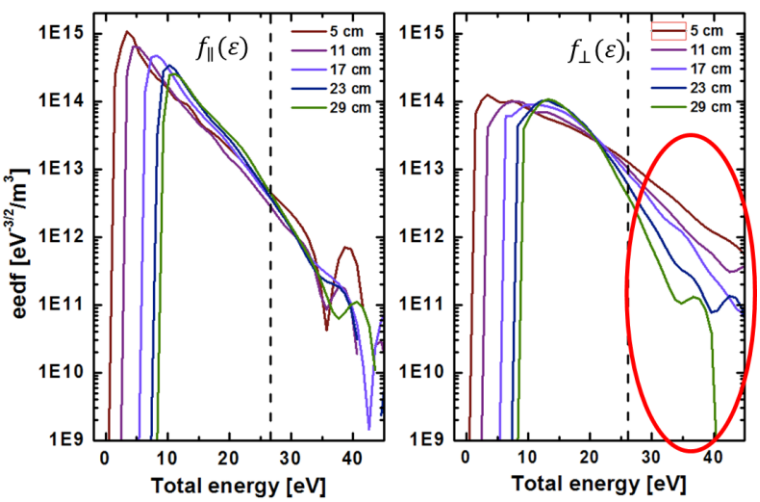

(b)

Figure 5.4 Electron energy distribution function for the overall energy shifted to match the same plasma potential reference in nozzle throat. (a) 300 W MW power, (b) 600 W MW power, significant escaping electron cooling of perpendicular energy distribution at high potential gradient region.

As shown in Fig. 5.5, in region 2, where the plasma is already adiabatic, the perpendicular electron energy cooling is relevant with the increasing power at the plasma source. There is also no significant difference in the energy distribution in the perpendicular and the parallel direction. Interestingly, however, in the case of high power, it is observed that in the trapped electrons, the parallel temperature does not cool along the magnetic field, but rather heats up and the temperature rises. As we have already seen in the spatial profile of the plasma potential, in the increasing the perpendicular electron temperature due to the MW power increase, which is expected to favor the potential gradient formation, rather the potential gradient is decreased because of the absolute plasma potential increase in the far-field region. This, in turn, causes the heating of the parallel electrons in the trapped electron group to be used to raise the potential, thus disturbing the build-up of the total potential gradient.

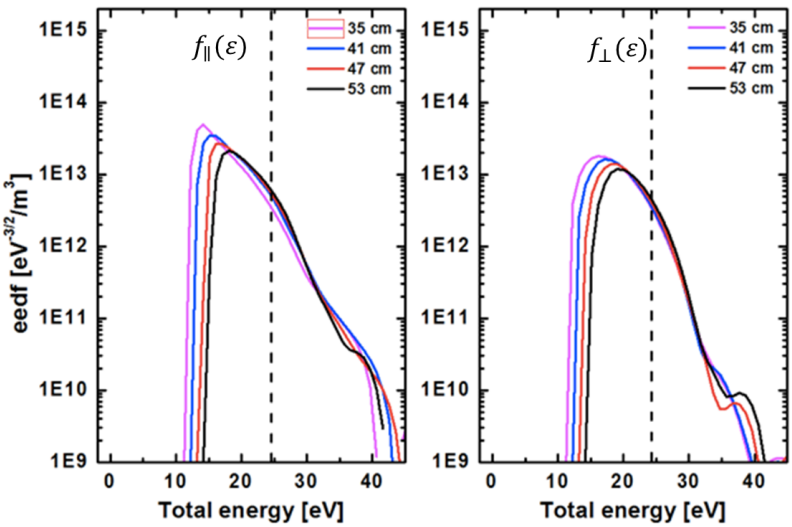

(a)

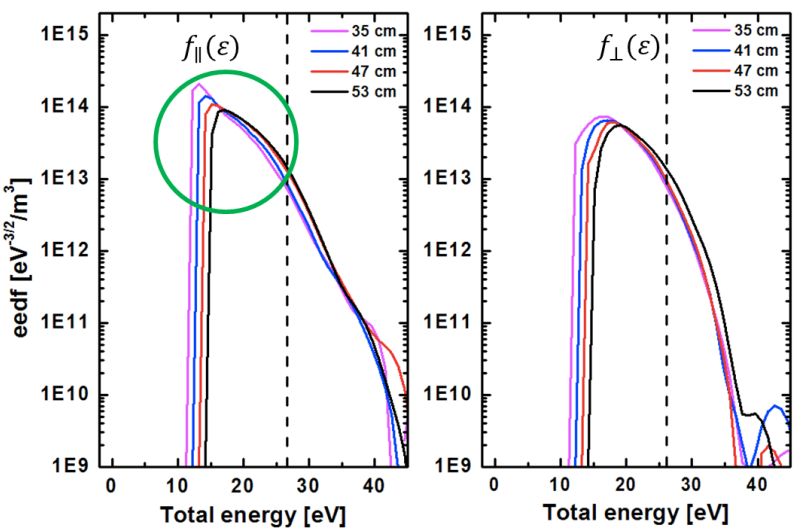

(b)

Figure 5.5 Electron energy distribution function for the overall energy shifted to match the same plasma potential reference in far-field region. (a) 300 W MW power, (b) 600 W MW power, Trapped electron heating of parallel energy distribution at low potential gradient region.

However, these results may be somewhat contradictory to the electron cooling in magnetically expanding plasma. In other words, it is observed that the electron in the parallel direction are heated by receiving the energy from the electrons in perpendicular direction, but the question remains that the cooling does not occur while expanding spatially. This can be understood as the relationship between the electric and magnetic fields in each the energy region.

In the case of electrons with low kinetic energy, the thermal conserved behavior can be explained by the balance of two opposite forces; force on electrons via electric field, $F_E = -e\nabla V_{\mathrm{p}}$, and inverse magnetic mirror effects, $F_B = \varepsilon_{\perp}|\nabla \mathrm{B}|/B$, respectively. In the case of low energy electrons, shown in Fig 5.6, the magnetic expansion is limited by spatial confinement effect via balance between magnetic mirror force and electric force; thus, the trapped electrons with low thermal energy at the nozzle throat cannot do work on an electric field that can be defined as a flexible boundary.

In the case of the escaping electrons with high kinetic energy, we can expect that the electron demagnetization by the divergent magnetic field can play a leading role. Therefore, as predicted in the modeling suggesting various demagnetization processes in the diverging magnetic field the phenomena can be interpreted with the fact that the degree of demagnetization of particles in collisionless plasma is strongly related to the electron kinetic energy. In magnetically expanding plasmas, the broken condition of the conservation of magnetic moment of particle can be expressed as $B/\nabla_{\parallel}B \ll v_{\mathrm{z}}/f_{\mathrm{ce}}$, where v_{z} and f_{ce} are the electron drift velocity in z-direction, and the electron cyclotron frequency, respectively. This relationship indicates that the drift scale length of electrons, $L_e = v_{\mathrm{z}}/f_{\mathrm{c,e}}$, during the characteristics scale length of the magnetic field inhomogeneity, $L_B = B/\nabla_{\parallel}B$, can be dependent on the average electron drift velocity. Therefore, it can be seen that the high energy group with shifted EEPFs produced via EEPF control shows thermal energy conservation with relatively larger non-adiabaticity parameter, L_e/L_B.

In summary, the electrons in the energy range below 10 eV near the nozzle throat are more subject to the electric field forces than to the magnetic mirror forces. It induces the trapped state while not expanding along the magnetic field. Without the cooling by the

adiabatic expansion, it is trapped and bounced in the electric field. The parallel electrons are thermalized by receiving the energy from the electrons in the perpendicular direction. It can be understood that the parallel electrons are heated in the EEDF measured from the experiment. Although not very low, the electrons with the energy lower than the wall potential is trapped because they do not overcome the potential barrier, but they are sufficiently affected by the magnetic field and are cooled by the adiabatic expansion. The electron energy group higher that potential barrier can escape and be cooled while expanding magnetically. However, in the far-field region where the magnetic field weakens and is separated from the magnetic field, the electron cooling will rarely occur.

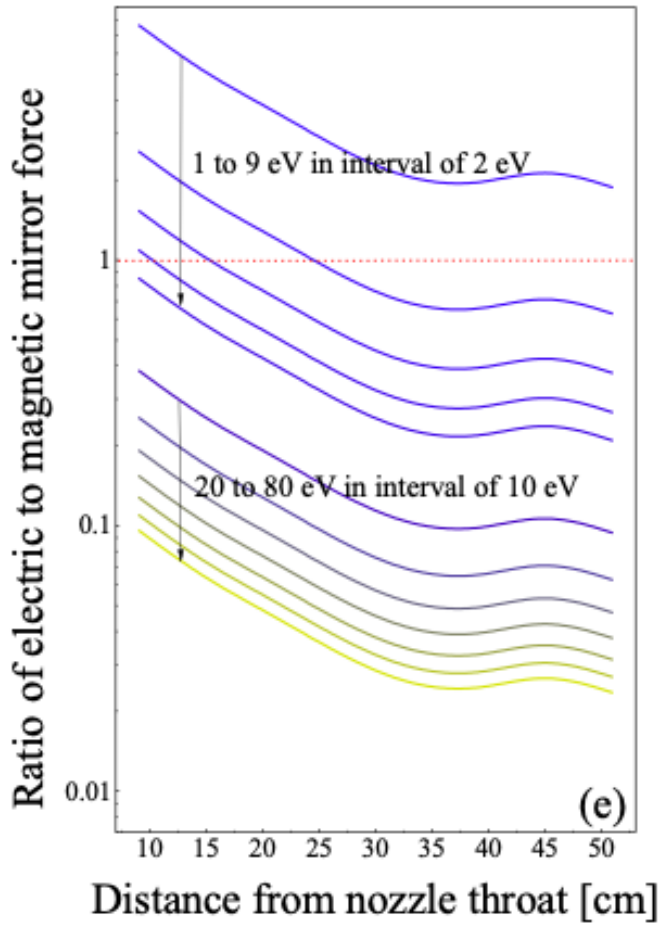

Figure 5.6 Axial profiles of ratio of electric to magnetic mirror force experienced by each the electron energy band.

The results calculated using the electron temperature and the potential measurements as to whether the total energy conservation perspective in the magnetic nozzle is experimentally correct, are shown in Fig. 5.7. The sum of the parallel electron temperature, twice perpendicular electron temperature in consideration of the two perpendicular directions and the potential energy may be referred to as total electron energy. If this value is normalized from the nozzle throat, it is not fixed to 1 along the axial magnetic field. That is, it means that the energy is not conserved along the magnetic nozzle. The difference between each calculation and 1 is the unknown energy consumed somewhere. In region 1, the unknown energy level increases as the power increases while expanding magnetically. No matter how heated the escaping electrons in the perpendicular direction contribute to the potential, they consume the energy elsewhere. On the other hand, the transfer to the unknown energy is similar even if it expands to region 2 when the power increases. As a result, the electron heating in the parallel direction serves to suppress the potential formation. The cooling and heating of the kinetic electron group in both directions are quantitatively expressed from the changes in the slope of EEDF, and the energy transfer path in each direction is arranged in Table 5.1 and Table 5.2.

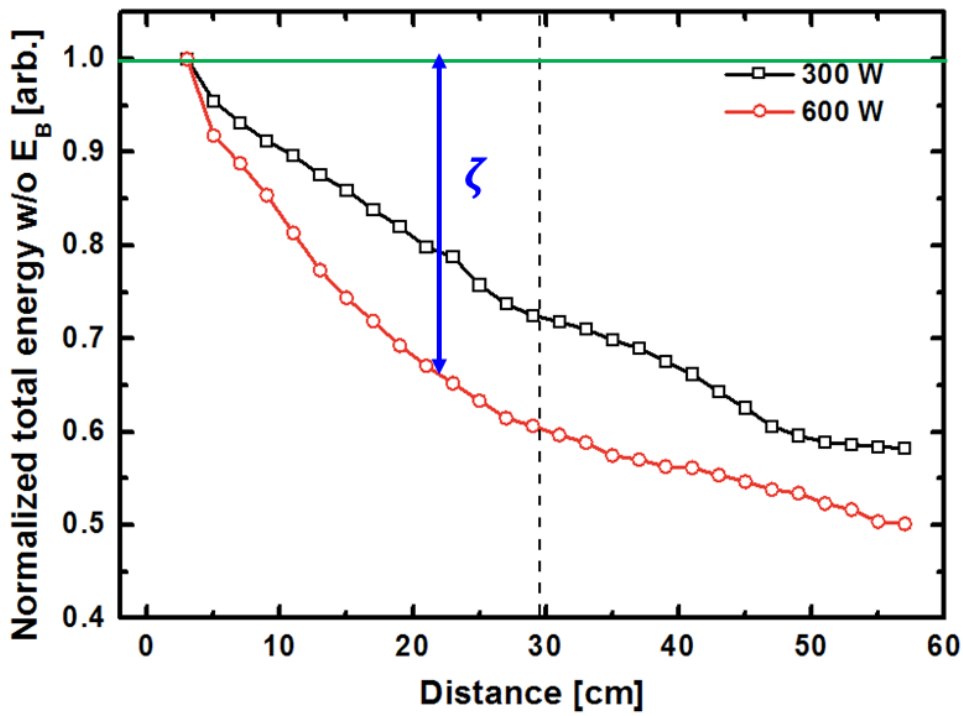

Figure 5.7 Normalized total energy which is a sum of measured thermal and potential energy.

Table 5.1 Quantitative energy cooling and heating of each electron group according to the energy region of kinetic electrons, and possible path of electron energy transfer in each direction in near-nozzle (Region 1).

Region 1	Low power (300 W)	High power (600 W)
$T_{\perp,e}$	Low energy region • Trapped electrons • Cooling (42%) • $E_{\perp} \rightarrow E_{\parallel}, e\phi$	Low energy region • Trapped electrons • Cooling (49%) • $E_{\perp} \rightarrow E_{\parallel}, e\phi$
	High energy region • Escaping electrons • Cooling (28%) • $E_{\perp} \rightarrow E_{\parallel}, \zeta$	High energy region • Escaping electrons • **Significant cooling (65%)** • $E_{\perp} \rightarrow E_{\parallel}, \zeta$
$T_{\parallel,e}$	Low energy region • Trapped electrons • Weak cooling (15%) • $E_{\parallel} \rightarrow e\phi$	Low energy region • Trapped electrons • Weak cooling (17%) • $E_{\parallel} \rightarrow e\phi$
	High energy region • Escaping electrons • Cooling (20%) • $E_{\parallel} \rightarrow \zeta$	High energy region • Escaping electrons • Cooling (33%) • $\boldsymbol{E_{\parallel}} \rightarrow \zeta$

Table 5.2 Quantitative energy cooling and heating of each electron group according to the energy region of kinetic electrons, and possible path of electron energy transfer in each direction in far-field (Region 2).

Region 2	Low power (300 W)	High power (600 W)
$T_{\perp,e}$	Low energy region • Trapped electrons • Weak cooling (2%) • $E_{\perp} \rightarrow E_{\parallel}, e\phi$	Low energy region • Trapped electrons • Week cooling (2%) • $E_{\perp} \rightarrow E_{\parallel}, e\phi$
	High energy region • Escaping electrons • Weak cooling (10%) • $E_{\perp} \rightarrow E_{\parallel}, \zeta$	High energy region • Escaping electrons • Cooling (13%) • $E_{\perp} \rightarrow E_{\parallel}, \zeta$
$T_{\parallel,e}$	Low energy region • Trapped electrons • Weak heating (11%) • $E_{\parallel} \rightarrow e\phi$	Low energy region • Trapped electrons • **Heating (55%)** • $\boldsymbol{E_{\parallel} \rightarrow e\phi}$
	High energy region • Escaping electrons • Cooling (23%) • $E_{\parallel} \rightarrow \zeta$	High energy region • Escaping electrons • Weak cooling (9%) • $E_{\parallel} \rightarrow \zeta$

5.3 Evidence of Electric Potential Build-up by Trapped Electron Group

We divided thermodynamically the trapped and escaping electron groups from EEDF to investigate what characteristics each group had in the perpendicular and parallel directions. Based on the total energy conservation perspective, it was found that trapped electrons contributed to the potential gradient formation, and escaping electrons could interfere with the potential gradient formation, depending on the electron temperature anisotropy. This insight can be compared with the linear relationship between the change rate of the electron potential and the change rate of the perpendicular electron temperature via the polytropic index. The normalized plasma potential profiles obtained from the experimental measurements is shown in Fig. 5.8. As shown in Fig. 5.9, the potential change calculated by the total perpendicular electron temperature change rate, the sum of trapped and escaping, is very different from the measured potential change. On contrary, if we calculate the change of the plasma potential by the change of the electron temperature when the adiabatic expansion with the trapped electron group only as expected, it can be seen that it is similar to the profile of the plasma potential measured in the actual experiments as shown in Fig. 5.10. This validates the model that trapped electrons contribute to the potential build-up for the ion acceleration.

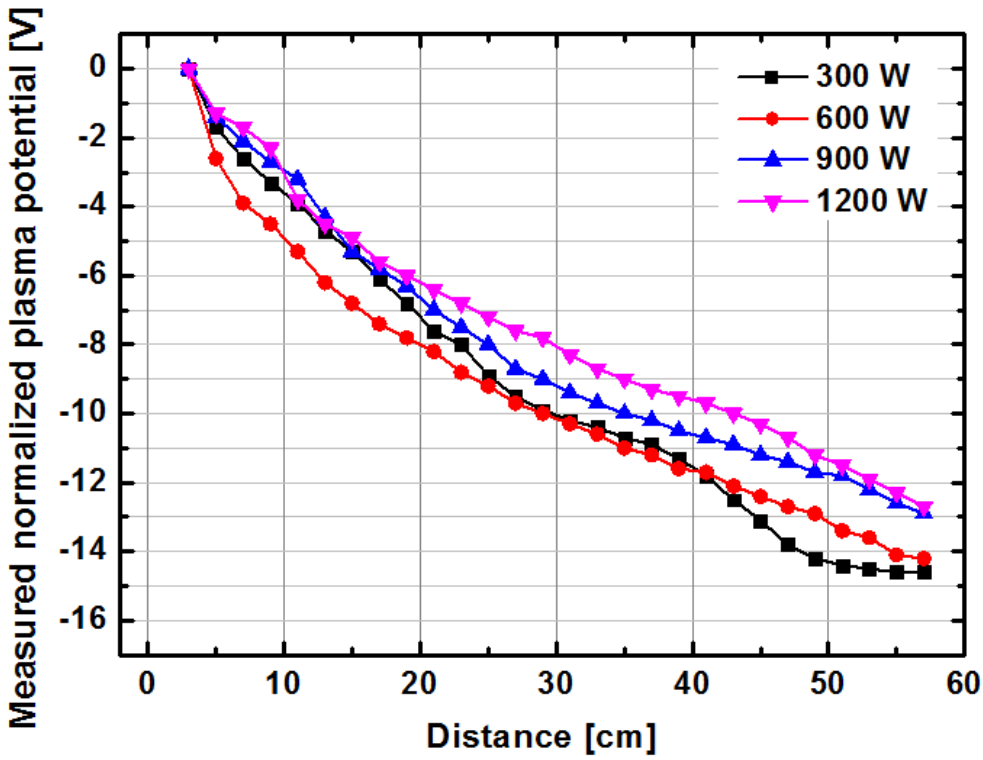

Figure 5.8 Normalized axial plasma potential profiles measured by experiments.

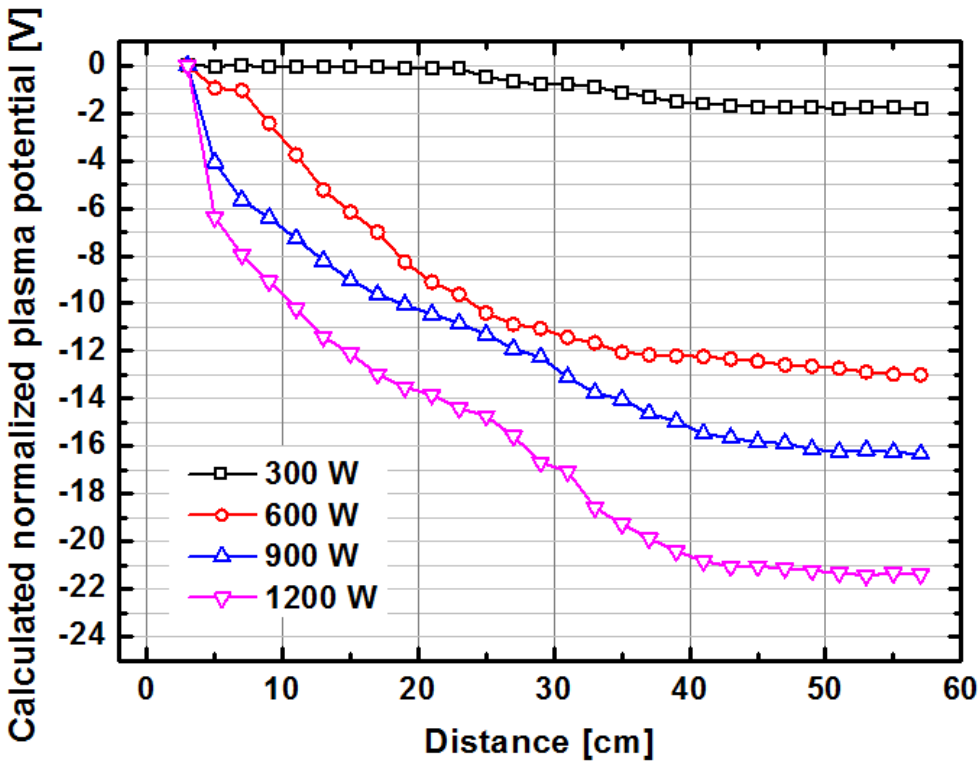

Figure 5.9 Normalized axial plasma potential profiles calculated by effective perpendicular electron temperature with $\gamma = 5/3$ including total trapped and escaping electron groups.

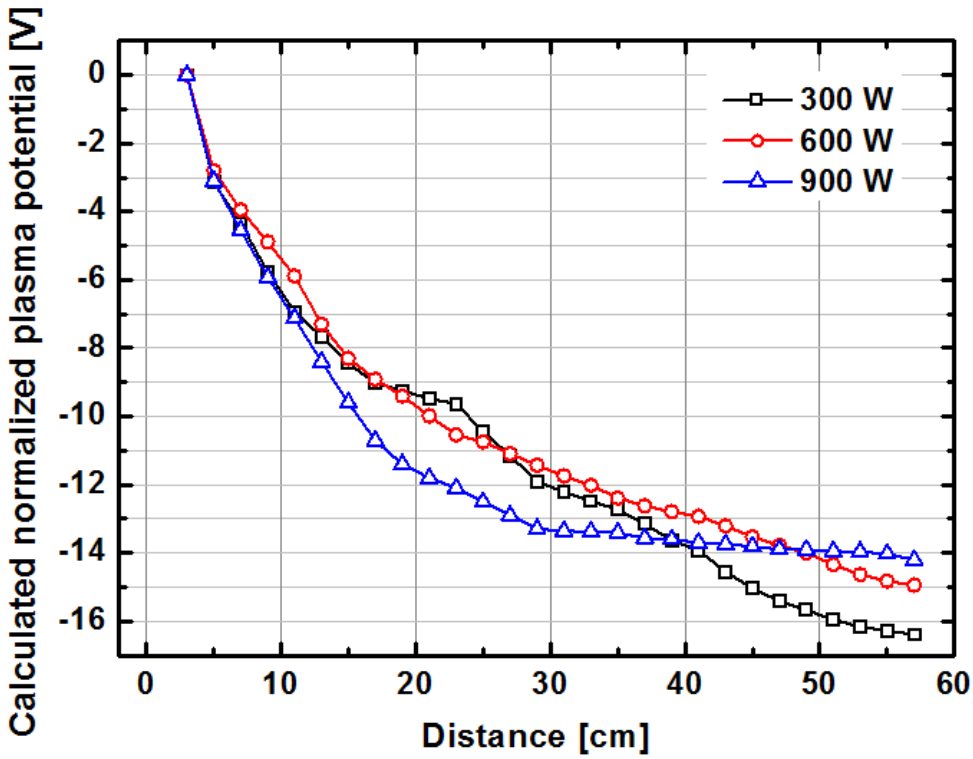

Figure 5.10 Normalized axial plasma potential profiles calculated by effective perpendicular electron temperature with $\gamma=5/3$ including trapped electron groups only.

Chapter 6 Conclusion and Future Work

Since the electron heating rate according source power is dependent on electrons energy and its direction, the electron thermodynamic approach should not be fluid perspective. Anisotropy of electron temperature can directly affect magnetic nozzle efficiency when generating magnetic nozzle plasma by wave heating. In anisotropic electron thermodynamic conditions such as perpendicular heating in ECR, the degree of confined electron cooling in the perpendicular direction is important for efficient potential gradient formation for ion acceleration. From the experimental results, two phenomena are revealed; 1) The cooling of escaping electrons cannot contribute to the formation of the plasma potential structure. 2) The exchange of energy between the perpendicular and parallel directions can weaken the electric field in the far region of the nozzle. From the engineering point of view, in order to efficiently increase ion energy, it is emphasized that the ratio of trapped electron group should be prioritized through plasma potential control.

Further research on the plasma generation method through parallel electron energy heating (e.g. helicon discharge) suggests that the energy conversion from the perpendicular direction to the parallel direction can be minimized. Heated parallel energy may contribute fully to the generation of plasma potential structure.

Appendix I Effective Polytropic Index

Theoretical studies on the plasma expansion in the magnetic nozzle have typically employed with an assumption as the Boltzmann relation that the electrons are isothermal. The relation is defined as follows,

$$n_e = n_0 \exp\left[\frac{V - V_0}{T_e}\right] \ . \qquad \text{(AII. 1)}$$

However, it is not obvious that the assumption with the constant spatial electron temperature for the computational advantage can be satisfied in the real anisotropic plasmas. Although the energy balance equation is accurate, the polytropic relation stands for the equation of state can easily represent the thermodynamic state of the magnetically expanding plasma. The heat flow defined by introducing a thermodynamic equation of state, $p = p(n, T)$ for the plasma. The equation can be represented as $p_e V^{\gamma} = C,\ p \cong p_e = C n_e^{\gamma}$. The quantity γ, called by polytropic index or adiabatic component, means how much the plasma temperature increases with compression.

From the equation of state for the adiabatic plasma which is not exchange the energy with their surroundings, if the electron is Maxwellian, $p_e = n_e T_e$, the first derivation is

$$\frac{d}{dt}\left(T_e n_e^{1-\gamma}\right) = 0 \ , \qquad \text{where } \frac{d}{dt} = \frac{\partial}{\partial t} + (\boldsymbol{v} \cdot \nabla) \ . \qquad \text{(AII. 2)}$$

An internal thermal energy ε in the low temperature plasma, defined the electron temperature with a degree of freedom *N* equals

$$\varepsilon = \frac{N}{2} T_e = \frac{1}{\gamma - 1} T_e \ , \qquad \text{(AII. 3)}$$

where $\gamma = (N + 2)/N$. From the equations (AII.2) and (AII.3), it can rearrange the differential as follows,

$$\frac{d}{dt}\left(\varepsilon n_e^{1-\gamma}\right) = 0 \ . \tag{AII.4}$$

The thermal energy is sum of perpendicular electron energy $\varepsilon_\perp$ and parallel electron energy $\varepsilon_\parallel$. The equation (AII.4) is can be summarized to the polytropic index in terms of the thermal energy, electron density, and each rate of change as following,

$$\gamma = 1 + \frac{d\varepsilon/dt}{\varepsilon}\frac{n}{dn/dt} \ . \tag{AII.5}$$

The derivative values in the polytropic index can be determined by the continuity, induction and double-adiabatic equation. First of all, from the continuity equation,

$$\frac{\partial n}{\partial t} + \nabla \cdot (n\boldsymbol{v}) = S \ , \tag{AII.6}$$

if the source term is negligible, the density change rate for the electron density is as follows,

$$\frac{1}{n}\frac{dn}{dt} = -\nabla \cdot \boldsymbol{v} \ . \tag{AII.7}$$

Second, assuming that the plasma is tied to the magnetic field line, the flux is frozen into the plasma. Consider a simple case, $\boldsymbol{B} = B_\parallel \hat{t}$ and $\boldsymbol{v} = v_\perp \hat{t} + v_\parallel \hat{t}$. From the induction equation as following,

$$\frac{\partial \boldsymbol{B}}{\partial t} = \nabla \times (\boldsymbol{v} \times \boldsymbol{B} - \eta \nabla \times \boldsymbol{B}) \ , \tag{AII.8}$$

magnetic Reynolds number can be defined as follows,

$$\mathfrak{R}_m = \frac{|v \times B|}{|\eta \nabla \times B|} \ . \tag{AII.9}$$

In case of the ideal MHD ($\mathfrak{R}_m \gg 1$), the convective term dominates and diffusion term is negligible. This is called perfectly conducting regime. In the conditions, applying the vector analysis, it is as follows,

$$\frac{\partial \boldsymbol{B}}{\partial t} = \nabla \times (\boldsymbol{v} \times \boldsymbol{B}) = \boldsymbol{v}(\nabla \cdot \boldsymbol{B}) - \boldsymbol{B}(\nabla \cdot \boldsymbol{v}) + B \cdot \nabla \boldsymbol{v} - \boldsymbol{v} \cdot \nabla \boldsymbol{B} \ , (\text{AII}.10-1)$$

$$\frac{d\boldsymbol{B}}{dt} = \frac{\partial \boldsymbol{B}}{\partial t} + \boldsymbol{v} \cdot \nabla \boldsymbol{B} = -\boldsymbol{B}(\nabla \cdot \boldsymbol{v}) + (\boldsymbol{B} \cdot \nabla)\boldsymbol{v}, \qquad (\text{AII}.10-2)$$

$$\boldsymbol{B} \cdot \frac{d\boldsymbol{B}}{dt} = -B^2(\nabla \cdot \boldsymbol{v}) + \boldsymbol{B} \cdot (\boldsymbol{B} \cdot \nabla)\boldsymbol{v}, \qquad (\text{AII}.10-3)$$

$$\frac{1}{B}\frac{d\boldsymbol{B}}{dt} = -(\nabla \cdot \boldsymbol{v}) + \frac{\boldsymbol{B}}{B^2} \cdot (\boldsymbol{B} \cdot \nabla)\boldsymbol{v}, \qquad (\text{AII}.10-4)$$

$$\frac{d\boldsymbol{B}}{dt} = -B\nabla \cdot \boldsymbol{v} + B\nabla_{\parallel} \cdot v_{\parallel} = -B\nabla_{\perp} \cdot v_{\perp} \ . \qquad (\text{AII}.10-5)$$

And then, the equation is arranged the following equation,

$$\frac{d\boldsymbol{B}}{dt} + \nabla \cdot (\boldsymbol{B} \cdot \boldsymbol{v}) = 0 \ , \qquad (\text{AII}.11)$$

in a form similar to the mass conservation equation. Therefore, in ideal MHD, magnetic field moves as if the magnetic flux is frozen-in the plasma. With convective derivative, two similar equations are

$$\frac{d\boldsymbol{B}}{dt} + \cdot \boldsymbol{B}\nabla_{\perp} v_{\perp} = 0 \ , \qquad (\text{AII}.12)$$

$$\frac{d\rho}{dt} + \cdot \rho\nabla_{\perp} v_{\perp} = 0 \ , \qquad (\text{AII}.13)$$

which result in

$$\frac{1}{\boldsymbol{B}}\frac{d\boldsymbol{B}}{dt} = \frac{1}{\rho}\frac{d\rho}{dt} = -\nabla_{\perp} \cdot v_{\perp} \ . \qquad (\text{AII}.14)$$

Third, the frozen-in field which is the field line cannot move across the plasma due to the strong coupled state, is in the condition of strongly magnetized plasma. In other words, the

plasma is anisotropic. If the compression of system happen slowly enough with a time scale, first adiabatic invariant, $\mu = mv_{\perp}^2/2B$ is conserved. The adiabatic invariants of particle motion in the strong magnetic field can be used to derive generalizations of following relationships for the case of compression that involves components both parallel and perpendicular to the magnetic field [66],

$$p_{\perp} = mn\left\langle\frac{v_{\perp}^2}{2}\right\rangle = n\langle\mu\rangle B \quad . \tag{AII. 15}$$

If the compression is fast compared to collisions, but slow compared to Larmor gyration of the particles, magnetic moment of each particle will be conserved as follows,

$$\frac{d}{dt}\left(\frac{p_{\perp}}{nB}\right) = 0 \quad . \tag{AII. 16}$$

It is a meaningful formula which is from the adiabatic invariant of single particle to equation of state in terms of macroscopic variables in the field description. For examples, in case of the pure transversal compression as shown Fig. A.1(a), the conservation of particles and magnetic flux are satisfied (n $\propto$ B), assuming that the parallel length $L_{\parallel}$ is constant. The result is follows,

$$\frac{d}{dt}\left(\frac{p_{\perp}}{n^2}\right) = 0 \quad , \tag{AII. 17}$$

then the polytropic index is 2, that means 2-D adiabatic compression. On the other hand, in case of the pure longitudinal compression as shown Fig. A.1(b), the particles and magnetic flux are conserved in condition of as follows,

$$L_{\parallel} = \frac{V}{A} \propto \frac{B}{n} \quad . \tag{AII. 18}$$

That is satisfied as follow equation,

$$J = \int pdq = \int v_{\parallel} dl \cong v_{\parallel} L_{\parallel} \quad , \tag{AII. 19}$$

called by 2nd adiabatic invariant. And then, the resultant is follows,

$$\frac{d}{dt}\left(\frac{p_{\parallel}B^2}{n^3}\right) = 0 \ , \qquad \text{(AII. 20)}$$

then, the polytropic index is 3, for the pure parallel compression of the constant magnetic field intensity, that means 1-D adiabatic compression.

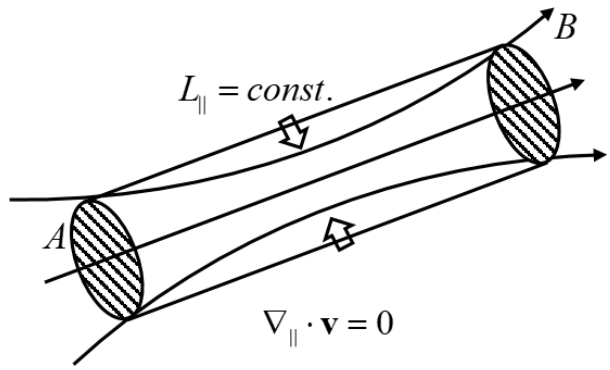

(a)

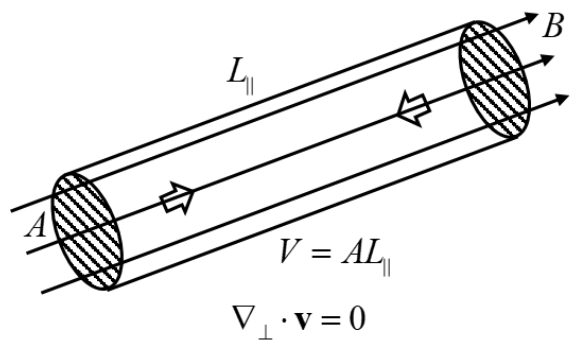

(b)

Figure A.1 Schematic illustration of (a) Pure transversal compression, (b) Pure longitudinal compression in the magnetic flux.

In order to illustrate the dependence of effective polytropic index on the temperature anisotropy and on the plasma flow, assume that the ionization is negligible. The derivations of density, magnetic field and internal energy are represented by the divergence of flow velocity as shown follows.

$$\frac{dn}{dt}+\nabla\cdot\left(n\mathbf{v}\right)=0 \longrightarrow \boxed{\frac{1}{n}\frac{dn}{dt}=-\nabla\cdot\mathbf{v}}$$

$$\frac{d}{dt}\left(\frac{\mathbf{B}}{\rho}\right)=\left(\frac{\mathbf{B}}{\rho}\cdot\nabla\right)\mathbf{v}=0 \longrightarrow \frac{d\mathbf{B}}{dt}+\nabla_{\perp}\cdot\left(B\mathbf{v}_{\perp}\right)=0 \longrightarrow \boxed{\frac{1}{B}\frac{dB}{dt}=-\nabla_{\perp}\cdot\mathbf{v}_{\perp}}$$

$$\frac{d}{dt}\left(\frac{p_{\perp}}{nB}\right)=0 \longrightarrow \frac{d}{dt}\left(\frac{v_{\perp}^{2}}{B}\right)=\frac{d}{dt}\left(\frac{\varepsilon_{\perp}}{B}\right)=0$$

$$\longrightarrow \frac{d}{dt}\left(\frac{\varepsilon_{\perp}}{B}\right)=\left(\frac{\varepsilon_{\perp}}{B}\cdot\nabla\right)\mathbf{v}=0 \longrightarrow \left(\frac{d\varepsilon_{\perp}}{dt}+\nabla_{\perp}\cdot\left(\varepsilon_{\perp}\mathbf{v}_{\perp}\right)=0\right)\longrightarrow \boxed{\frac{1}{\varepsilon_{\perp}}\frac{d\varepsilon_{\perp}}{dt}=-\nabla_{\perp}\cdot\mathbf{v}_{\perp}}$$

$$\frac{d}{dt}\left(\frac{p_{\parallel}B^{2}}{n^{3}}\right)=0 \longrightarrow \frac{d}{dt}\left(\frac{B^{2}v_{\parallel}}{n^{2}}\right)=\frac{d}{dt}\left(\frac{B^{2}\varepsilon_{\parallel}^{1/2}}{n^{2}}\right)=0 \qquad \text{where } v_{\perp}^{2}\propto\varepsilon_{\perp},\ v_{\parallel}^{2}\propto\varepsilon_{\parallel}$$

$$\longrightarrow \frac{d}{dt}\left(\frac{B^{2}\varepsilon_{\parallel}^{1/2}}{n^{2}}\right)=\left(\frac{B^{2}\varepsilon_{\parallel}^{1/2}}{n^{2}}\cdot\nabla\right)\mathbf{v}=0 \longrightarrow \left(\frac{d\varepsilon_{\parallel}^{1/2}}{dt}+\nabla_{\parallel}\cdot\left(\varepsilon_{\parallel}^{1/2}\mathbf{v}_{\parallel}\right)=0\right)\longrightarrow \boxed{\frac{1}{\varepsilon_{\parallel}}\frac{d\varepsilon_{\parallel}}{dt}=-2\nabla_{\parallel}\cdot\mathbf{v}_{\parallel}}$$

Finally, the effective polytropic index is derived as follows,

$$\begin{aligned}\gamma_{eff}&=1+\frac{d\varepsilon/dt}{\varepsilon}\frac{n}{dn/dt}=1+\frac{\left(d\left(\varepsilon_{\perp}+\varepsilon_{\parallel}\right)/dt\right)/\left(\varepsilon_{\perp}+\varepsilon_{\parallel}\right)}{\left(dn/dt\right)/\mathrm{n}}\\&=1+\frac{\varepsilon_{\perp}\nabla_{\perp}\cdot v_{\perp}+2\varepsilon_{\parallel}\nabla_{\parallel}\cdot v_{\parallel}}{\varepsilon\left(\nabla\cdot\mathbf{v}\right)}=1+\frac{1+\dfrac{2\varepsilon_{\parallel}\nabla_{\parallel}\cdot v_{\parallel}}{\varepsilon_{\perp}\nabla_{\perp}\cdot v_{\perp}}}{\left(1+\dfrac{\varepsilon_{\parallel}}{\varepsilon_{\perp}}\right)\left(1+\dfrac{\nabla_{\parallel}\cdot v_{\parallel}}{\nabla_{\perp}\cdot v_{\perp}}\right)}\\&=1+\frac{1+\dfrac{2\varepsilon_{\parallel}K_{\parallel}}{\varepsilon_{\perp}K_{\perp}}}{\left(1+\dfrac{\varepsilon_{\parallel}}{\varepsilon_{\perp}}\right)\left(1+\dfrac{K_{\parallel}}{K_{\perp}}\right)}=1+\frac{1+2\alpha\beta}{\left(1+\alpha\right)\left(1+\beta\right)}\end{aligned} \qquad . \qquad \text{(AII. 21)}$$

Bibliography

[1] R. G. Jahn, Physics of electric propulsion. (McGraw-Hill, New York, 1968).

[2] D. A. Kaufman, D. G. Goodwin, and J. C. Sercel, 29th Joint Propulsion Conference and Exhibit (1993).

[3] C. Charles and R. W. Boswell, Appl. Phys. Lett. 82, 9 (2003).

[4] R. W. Boswell and E. Marsch, and C. Charles, Astrophys. J. 640, L199 (2006).

[5] A. V. Arefiev and B. N. Breizman, Phys. Plasmas 15, 042109 (2008).

[6] C. Charles, J. Phys. D 42, 16 (2009).

[7] O. V. Batishchev, IEEE Trans. Plasma Sci. 37, 8 (2009).

[8] B.W. Longmier et al., Plasma Sources Sci. Technol. 20, 015007 (2011).

[9] D. M. Goebel and I. Katz, Fundamentals of Electric Propulsion: Ion and Hall Thrusters (Wiley, New York, 2008).

[10] I. Levchenko et al., Nature Communications 9, 879 (2018).

[11] A. V. Arefiev and B. N. Breizman, Phys. Plasmas 16, 055707 (2009).

[12] E. Ahedo and J. N. Cavalle, Phys. Plasmas 20, 043512 (2013).

[13] M. Merino and E. Ahedo, IEEE Trans. Plasma Sci. 43, 1 (2015).

[14] R. Hoyt et al., IEEE Trans. Plasma Sci. 23, 481 (1995).

[15] K. Schoenberg, et al., Phys. Plasmas 5, 2090 (1998).

[16] Ebersohn, F. H. Ph. D. thesis; Texas A&M University (2012).

[17] Olsen et al., IEEE Trans, Plasma Sci, 43 252-68 (2015).

[18] J. P. Sheehan et al., Plasma Sources Sci. Technol. 23, 045014 (2014).

[19] S. A. Cohen et al., Rev. Sci. Instrum. 61, 11 (1990).

[20] Cohen S A et al., Phys. Plasmas 10, 2593 (2003).

[21] K. Takahashi et al., Phys. Rev. Lett. 107, 235001 (2011).

[22] K. Takahashi, A. Chiba, A. Komuro, and A. Ando, Phys. Rev. Lett. 114, 195001 (2015).

[23] K. Takahashi and A. Ando, Plasma Phys. Control. Fusion 59, 054007 (2017).

[24] C. Charles and R. W. Boswell, Appl. Phys. Lett. 82, 1356 (2003).

[25] C. Charles, Plasma Sources Sci. Technol. 16, R1 (2007).

[26] J. M. Little and E. Y. Choueiri, Phys Rev. Lett. 117, 225003 (2016).

[27] J. M. Little, Ph.D. thesis, Princeton University (2015).

[28] G. Sanchez-Arriaga, J. Zhou, E. Ahedo, M. Martinez-Sanchez, and J. Ramos, Plasma Sources Sci. Technol. 27, 035002 (2018).

[29] S. A. Andersen, V. O. Jensen, P. Nielsen, and N. D'Angelo, Phys. Fluids 12, 557 (1969).

[30] M. A. Raadu, Plasma Phys. 21, 331 (1979).

[31] M. Dryer, J. Geophys. Res. 76, 4 (1971).

[32] S. A. Andersen, V. O. Jensen, P. Nielsen, and N. D'Angelo, Phys. Fluids 12, 557 (1969).

[33] M. A. Raadu, Plasma Phys. 21, 331 (1979).

[34] M. Dryer, J. Geophys. Res. 76, 4 (1971).

[35] E. Ahedo, M. Merino, Phys. Plasmas 18, 053503 (2011).

[36] J. Navarro-Cavalle, S. Correyero, and E. Ahedo, Proceedings of 34th International Electric Propulsion Conference, Kobe, Japan, July 4 –10, 2015, IEPC-2015-117 (IEPC, Kobe, 2015).

[37] M. Merino and E. Ahedo, IEEE Trans. Plasma Sci. 43, 1 (2015).

[38] J. Y. Kim et al., Plasma Sources Sci. Technol. 28, 07LT01 (2019).

[39] K. Takahashi, C. Charles, R. W. Boswell, A. Ando, Phys. Rev. Lett. 120, 045001 (2018).

[40] Y. Hu, J. Wang, IEEE Trans. Plasma Sci. 43, 9 (2015).

[41] S. Correyero et al., AIAA Pro. Ener. (2016).

[42] K. S. Chung et al., Fusion Eng. Des. 109, 454 (2016).

[43] V. A. Godyak, and V. I. Demidov. J. Phys D: Appl. Phys. 44, 233001 (2011).

[44] G. F. Matthews et al., Plasma Phys. Controlled Fusion 32, 1301 (1990).

[45] T. Shikama et al., Phys. Plasmas 21, 073510 (2014).

[46] R. C. Wood and I. D. Sudit Phys. Rev. E 50 (1994).

[47] R. B. Lobbia and B. E. Beal, Journal of Propulsion and Power, 33, 3 (2017).

[48] J. Y. Kim et al., New J. Phys. 20, 063033 (2018).

[49] J. Navarro-Cavalle, S. Correyero, and E. Ahedo, Proceedings of 34th International Electric Propulsion Conference, Kobe, Japan, July 4 –10, 2015, IEPC-2015-117 (IEPC, Kobe, 2015).

[50] R. W. Boswell, K. Takahashi, C. Charles and I. D. Kaganovich, Front. Phys. 3, 14 (2015).

[51] K. Terasaka, et al., Physics of Plasmas 17, 072106 (2010).

[52] M. Merino, Ph. D. Thesis (2013).

[53] Y. Hu, J. Wang, Phys. Plasma 24, 033510 (2017).

[54] K. Terasaka et al, J. Plasma Physics 81 (2015).

[55] E. B. Hooper, Journal of Propulsion and Power 9, 5 (1993).

[56] K. Kuriki and O. Okada, Phys. Fluids 13, 9 (1970).

[57] C. Charles and R. W. Boswell, Phys. Plasma 11, 4 (2004).

[58] P. Balan et al., Contrib. Plasma Phys. 44, 7-8 (2004).

[59] S. Samukawa, Jpn. J. Appl. Phys. 31 (1992).

[60] M. Merino and E. Ahedo, Plasma Sources Sci. Technol. 25, 045012 (2016).

[61] M. Merino and E. Ahedo, Phys. Plasma 23, 023506 (2016).

[62] M. Merino et al., Plasma Sources Sci. Technol. 24, 035006 (2015).

[63] A. Fruchtman, et al., Phys. Plasma 19, 033057 (2012).

[64] G. Manfredi, et al., Phys. Fluids B 5 (1993).

[65] M. Pudovkin et al., J. Geophys. Reserch 102, A12 (1997).

[66] G. Chew, M. Goldberger and F. Low, Proc. Roy. Soc. A 236, 112 (1956).

Abstract in Korean

자기적으로 팽창하는 플라즈마에서의 구속된 전자에 의한 양극성 전위 형성 연구

정경수

에너지시스템공학부

(핵융합 및 플라즈마 공학 전공)

서울대학교 대학원

자기 노즐은 팽창하는 자기장 속에서 플라즈마 전자의 단열 팽창에 의하여 가속된 이온 빔을 추력에 활용하는 개념으로써, 이온 빔 중성화를 위한 음극의 추가적인 설치 없이 팽창하는 전자를 직접 중성화에 활용할 수 있다는 장점이 있어 차세대 전기 추력기로써의 가능성을 주목 받고 있다. 이온 빔 가속 에너지 관점에서 자기 노즐 장치의 효율은 폴리트로픽 방정식 (polytropic equation)을 통한 자기 단열 팽창에 의한 전자 냉각과 플라즈마 전위 구배의 관계에 의하여 결정된다. 따라서 자기노즐 장치에서 전자의 열역학적 상태에 대한 명확한 이해는 추력 효율에 직접적으로 기여한다는 중요성 아래 다양한 연구들이 수행되어 왔다.

자기 노즐 플라즈마에서의 전자 열역학적 상태에 대한 해석을 위해서는 전자 가스 계(system) 내부 에너지의 변화가 유동 주변부 (flexible surrounding)으로 정의된 자기장 및 전기장에 일을 수행한다는 전체 에너지 보존 법칙을 도입하여 자기적으로 팽창하는 플라즈마를 모사한다. 이 때 전자 열역학적 상태에 대한 기존 연구 그룹들의 실험 및 모델링 결과들은 플라즈마 내부에 존재하는 전위 장벽 혹은 자기 모멘트에 의한 전자 구속 여부를 기준으로 하여 시스템을 양분할 수 있게 한다. 전기적으로 구속된 전자 (trapped electrons)의 경우 전자의 단열 팽창은 전기장 구조 형성에 기여하는 반면, 탈출 전자 (escaping electrons)는 자기장 구조의 변경을 야기시키는 일을 할 수 있다. 따라서 자기 노즐 플라즈마에서의 전자의 열역학적 상태는 정전기적 구속 상태의 고려가 필수적임을 암시한다. 전자계의 명확한 정의를 바탕으로 한 열역학적 상태 규명에 집중하여 수행된 선행연구들은 전자의 열역학적 상태와 자기 노즐의 효율간의 관계 연구에 대한 기반이 되었으며, 복잡한 플라즈마 물리 특성을 반영한 세분화된 연구를 필요로 한다.

자기 노즐 장치에서 플라즈마 생성이 전자의 에너지 및 방향 선택적 가열에 의하여 달성된다는 점에 착안하여, 전자의 열역학적 상태 변화에 의한 플라즈마 전위 구배 형성 연구가 전자의 방향성을 고려한 진단을 바탕으로 수행되어야 함을 강조한다. 이를 위하여 전자 공명 가열(electron cyclotron resonance) 방식을 통한 플라즈마 생성원에서 인가 전력을 증가시켜 선택적으로 전자의 수직 방향 에너지를 변화시키면서 전자의 각 방향 성분 (자기장에 대해 수직과 수평) 의 전자 에너지 분포 함수 측정을 통하여 전자 열역학적 특성과 플라즈마 전위 구배 형성에 관한 연구를 수행한다. 흥미롭게도, 노즐 입구에서 전자의 수직 에너지 증가는 플라즈마 전위 구배 형성에 기여하지 못하였으며, 이는 전자 가열을 위하여 인가된 전력의 대부분이 탈출 전자의 수직 방향 에너지 상승에 기여했기 때문으로 해석된다. 수평 방향의 전자 에너지의 경우, 인가 전력이 증가 됨에 따라 노즐의 먼

영역에서 가열되는 특성이 관찰 되었으며, 이러한 가열은 플라즈마 전위의 절대값의 상승 효과를 일으켜 수직 방향의 구속 전자 그룹에 의하여 생성된 양극성 전기장을 감쇠하는데 영향을 주었다. 인가 전력에 따른 구속 전자의 수직 방향 성분으로부터 수평 방향 성분으로의 에너지 전달과 냉각을 포함한 변화와 플라즈마 전위 구배 변경 간의 상관관계는 구속된 전자가 단열 팽창을 통하여 전기장 형성에 기여 함을 증명 하였으며 다음과 같은 점들을 시사한다. 첫째, 전자 공명 가열을 활용한 자기 노즐 장치에서 이온 가속을 위한 전기장 형성에는 구속 전자의 가열이 직접적으로 이바지한다. 둘째, 구속 전자의 축 방향 열에너지의 변화와 전기장 변화는 폴리트로픽 지수가 5/3 에 가까운 단열 팽창으로 설명된다. 셋째, 수직방향과 수평방향 간의 전자 에너지 교환은 노즐의 먼 영역에서 전기장을 약화 시킬 수 있으며, 따라서 이를 반영한 자기 노즐 연구에서의 모델링과 장치 설계가 필수적이다.

본 연구는 웨이브 가열에 의한 자기 노즐 플라즈마 생성시 전자 온도의 비등방성이 자기 노즐 효율에 직접적인 영향을 줄 수 있음을 강조하는 최초의 연구이다. 공학적 관점에서 이온 에너지의 효율적인 상승을 위하여 플라즈마 전위 조절을 통한 구속 전자의 비율 증가가 우선 되어야함을 강조하며, 플라즈마 생성 영역에서 수평 방향 전자 에너지 가열을 통한 플라즈마 생성 방식에 대한 추가 연구를 통하여, 노즐의 먼 영역에서 자기 팽창에 따른 수직 방향에서 수평 방향으로의 에너지 전환이 최소화 될 수 있음을 암시한다.

주요어 : 자기노즐, 폴리트로픽 지수, 전자 냉각, 지향적 랑뮤어 탐침, 비등방적 전자 에너지 분포, 양극성 전위

학번 : 2013-30295